ChemBioChem

Review
doi.org/10.1002/cbic.202300044

Chemistry Europe
European Chemical Societies Publishing

www.chembiochem.org

Thiophene-Based Ligands: Design, Synthesis and Their Utilization for Optical Assignment of Polymorphic-Disease-Associated Protein Aggregates

Linnea Björk,[a] Therése Klingstedt,[a] and K. Peter R. Nilsson*[a]

The development of ligands for detecting protein aggregates is of great interest, as these aggregated proteinaceous species are the pathological hallmarks of several devastating diseases, including Alzheimer's disease. In this regard, thiophene-based ligands have emerged as powerful tools for fluorescent assessment of these pathological entities. The intrinsic conformationally sensitive photophysical properties of poly- and oligothiophenes have allowed optical assignment of disease-associated protein aggregates in tissue sections, as well as real-time in vivo imaging of protein deposits. Herein, we recount the chemical evolution of different generations of thiophene-based ligands, and exemplify their use for the optical distinction of polymorphic protein aggregates. Furthermore, the chemical determinants for achieving a superior fluorescent thiophene-based ligand, as well as the next generation of thiophene-based ligands targeting distinct aggregated species are described. Finally, the directions for future research into the chemical design of thiophene-based ligands that can aid in resolving the scientific challenges around protein aggregation diseases are discussed.

1. Introduction

Ligands targeting distinct pathological hallmarks are essential for detecting specific biomolecular entities and studying molecular events occurring during the pathogenesis of individual diseases, as well as for clinical diagnostics of distinct disorders. A pathological hallmark that is involved in the pathogenesis of several devastating diseases, including neurodegenerative diseases (NDs) such as Alzheimer's disease (AD) and Parkinson's disease (PD), as well as systemic amyloidosis, is aggregated proteins, so called amyloids.[1] These protein aggregates originate from different precursor proteins, but one thing they have in common is that they are rich in β-sheet structure and that these β-sheets arrange structurally in a repetitive pattern called the cross-β motif (Figure 1A).[2–6] As the aggregation process starts many years before the onset of clinical symptoms, especially in NDs,[7–11] the development of ligands selectively detecting these disease-associated protein aggregates is essential from a clinical perspective. A selection of ligands targeting the repetitive cross-β structure (Figure 1B) has been presented and these ligands can be used to detect protein aggregates in general.[12–14] However, even though all amyloids share this structural arrangement, a structural polymorphism has been observed for many disease-associated protein aggregates.[15–19]

The histopathological hallmarks of AD are extracellular plaques composed of the amyloid-β (Aβ) peptide and intracellular neurofibrillary tangles (NFTs) made of hyperphosphorylated tau. Despite these common histological features, the clinical and pathological phenotype of AD exhibit conspicuous variability among and within patients.[20–23] These heterogeneous phenotypes have been anticipated to occur due to the existence of distinct morphotypes of Aβ and tau aggregates.[24–28] The prion protein is a classic example of how an identical protein primary sequence can misfold into distinct aggregate morphotypes, so called prion strains, giving rise to specific neuropathological and clinical abnormalities.[29] A similar polymorphism has also been suggested for Aβ, since variations in Aβ aggregate morphology can be seen in transgenic mouse models with Aβ pathology and in AD patients.[30–34] Furthermore, seeding experiments in vitro and in mice have shown that the structure of the initial donor seed is self-propagated to the newly formed fibrils,[35,36] and when using Aβ aggregates extracted from AD patients with distinct disease phenotype for seeding, fibrils with different structures were also obtained.[37–39] Recently, cryogenic electron microscopy (cryo-EM) studies of Aβ fibrils prepared by seeded growth[40] or fibrils isolated from human brain tissue[41,42] have confirmed the existence of distinct Aβ aggregate morphotypes (Figure 1C). The structural properties of pathological tau filamentous inclusions have also been examined and such accumulations of tau are not only present in AD, but in a range of NDs referred to as tauopathies.[43] More than 20 years ago, transmission electron microscopy (TEM) studies showed that tau filaments isolated from the brains of different tauopathy cases exhibited a morphological variation.[44] More recently, the cryo-EM technique has enabled determination of high-resolution structures of

[a] L. Björk, Dr. T. Klingstedt, Prof. K. P. R. Nilsson
Department of Physics, Chemistry and Biology
Linköping University
581 83 Linköping (Sweden)
E-mail: peter.r.nilsson@liu.se

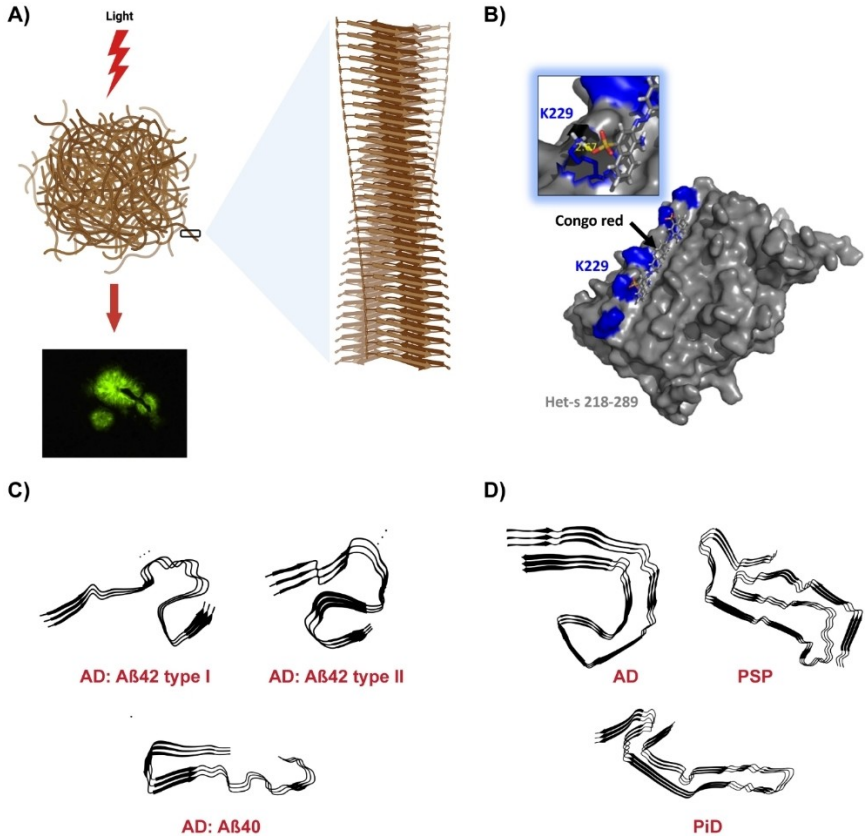

Figure 1. Polymorphic disease-associated protein aggregates. A) Schematic drawing of a protein aggregate composed of fibrils having β-sheets structurally arranged in a repetitive pattern called the cross-β motif; these aggregates can be visualized by using fluorescent ligands that bind to the cross-β sheet structure. The cross β-sheet structure is common to all protein aggregates and in each sheet, the β-strands are aligned perpendicular to the long axis of the amyloid fibril. The drawing was created with BioRender.com. B) HADDOCK model (Protein Data Bank (PDB) ID: 2LBU) of Congo Red docked to HET-s (218–289)E265 K based on NMR-derived distance restraints. One of the key residues, K229, interacting with anionic side-chain groups of the ligand, is marked in blue. C) The fold of the secondary structure elements in Aβ filaments extracted from the brain (Aβ42 type I and type II) or meninges (Aβ40) of patients with AD. The schematics were prepared by using PDB ID: 7Q4B (Aβ42 type I), 7Q4M (Aβ42 type II) or 6SHS (Aβ40). D) The fold of the secondary structure elements in the core of tau filaments purified from the brain of individual with AD, PSP or PiD. The schematics were prepared by using PDB ID: 5O3L (AD), 7P65 (PSP) or 6GX5 (PiD).

filamentous tau. The results have confirmed that the structures of tau filaments isolated from different tauopathy brain tissue samples, such as AD, progressive supranuclear palsy (PSP) and Pick's disease (PiD), are distinct, and that a classification of tauopathies based on tau filament structure can be achieved (Figure 1D).[45–49] Moreover, tau filaments assembled *in vitro* are structurally different compared to those derived from human brain tissue.[50] A structural difference between brain-derived filaments and those formed *in vitro* has also been reported for Aβ.[41,42]

In PD, the main constituent of the pathological deposits is the protein α-synuclein (α-syn), which forms neuronal accumulations termed Lewy bodies (LBs) and Lewy neurites (LNs).[51] Assemblies of α-syn are also present in the brain of patients with dementia with Lewy bodies (DLB) or multiple system atrophy (MSA). In the latter, the protein mainly accumulates in the oligodendrocytes forming glial cytoplasmic inclusions (GCIs).[52–54] When studied using TEM, the morphologies of α-syn filaments extracted from the brains of MSA patients have shown to be different from those derived from patients with PD or DLB.[52,55,56] The cryo-EM technique was recently applied on α-syn filaments isolated from the brains of patients with PD, DLB or MSA. In PD and DLB, the α-syn filaments were structurally identical,[57] whereas in MSA, two structurally different types of filaments were present.[58] Hence, similar to the observations for Aβ and tau aggregates, a structural polymorphism of α-syn assemblies has been shown.

Evidently, protein aggregates associated with NDs display a structural diversity and these proteins are also susceptible to a wide range of post-translational modifications. For example, serine and threonine residues can be phosphorylated and glycosylated, whereas lysine resides are subjected to acetylation, methylation and ubiquitylation, and such modifications are rather evident for tau.[59,60] Moreover, different versions of the Aβ peptide, such as Aβ 1–40 and Aβ 1–42, can be found in vascular and parenchymal Aβ deposits, respectively.[61–63] Such biochemical modifications can most likely also render structural variations of the proteinaceous aggregated species, as well as altering the binding mode of ligands targeting these pathological entities. Protein aggregates can also contain additional

molecules, such as heparan sulphate proteoglycan (HSPG) and serum amyloid P-component (SAP),[1] that might have an impact on the assembly of the deposits, as well as influence the binding mode of ligands. These so called "amyloid signature proteins" are common in amyloid deposits in systemic amyloidosis[1] and recently, cryo-EM studies have also revealed a structural polymorphism for protein aggregates associated with systemic amyloidosis.[64–70] Thus, polymorphic protein aggregates seems to be a common feature for several diseases and fluorescent ligands that can reveal and distinguish polymorphic protein aggregates would be essential for understanding the role of distinct aggregate morphotypes during the pathogenesis of specific diseases, as well as for accurate clinical diagnostics of individual disorders. In this regard, thiophene-based ligands have evolved as a class of fluorescent tools that can be utilized for optical assignment of disease-associated aggregates. In the next sections, we will give a brief history of the most conventional ligands that have been used for detection of protein aggregates, as well as exemplify the design, synthesis and use of thiophene-based ligands for optical assignment of polymorphic disease-associated protein aggregates.

2. Ligands for the Detection of Protein Aggregates: A Brief History

From a historical perspective, Congo red (CR), Thioflavin T (ThT) and derivatives thereof have been used as conventional ligands for the detection of protein aggregates having a typical repetitive pattern of cross-β structure. CR, an azo dye (Figure 2A), was discovered by accident in 1922 by Bennhold and is as of today the golden standard for amyloid detection.[71] In fact, one property required for the definition of amyloid is the green birefringence exhibited under polarized light from CR when bound to amyloid deposits.[1] Lately, it was shown that CR

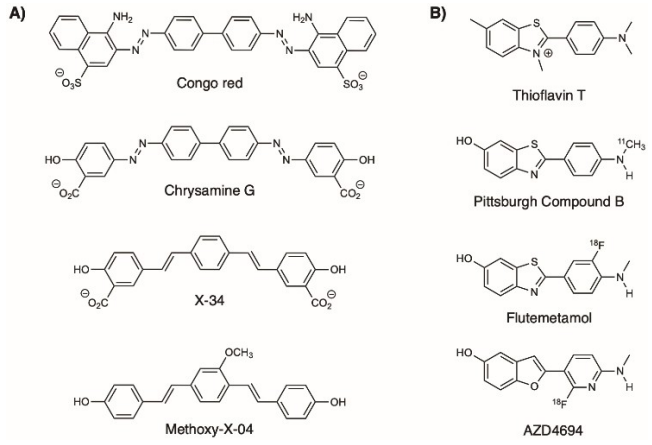

Figure 2. Different generations of Congo Red and Thioflavin T derivatives. A) Chemical structures of Congo Red (CR), Chrysamine G, X-34 and Methoxy-X-04. B) Chemical structures of ThT, Pittsburgh Compound B (PiB), Flutemetamol and AZD4694.

interacts with regularly spaced cationic lysine residues situated in well-accessible grooves along the protein aggregates (Figure 1B),[72] and several other derivatives, such as Chrysamine G,[73] X-34[74] and Methoxy-X-04,[75] of CR have been developed with the aim of improving the ligands' performance for identifying protein aggregates *in vitro* or *in vivo* (Figure 2A). For instance, X-34 is a highly fluorescent ligand that shows affinity for both Aβ and tau aggregates in histological applications.[74,76] In addition, Methoxy-X-04 has been useful for *in vivo* two-photon imaging of protein aggregates in transgenic mouse models.[75,77–79] However, despite several chemical modifications, CR derivatives have not shown the optimal properties for being used as efficient tracers for clinical imaging of protein aggregates with positron emission tomography (PET).[80]

In a similar fashion as CR, a variety of thioflavins have been used as ligands for protein aggregates. ThT (Figure 2B) was presented as a fluorescent ligand for amyloid detection in 1959 and has since then primarily been used for characterization of protein fibril formation *in vitro*.[81–83] Due to limited success of CR derivates as PET tracers for Aβ aggregates, the structure of ThT has also been optimized to achieve ligands for clinical diagnostics of AD.[80] The first example of a ligand that can be used for PET imaging of Aβ deposits in AD patients was Pittsburgh Compound-B (PiB),[84] a neutral lipophilic derivative of ThT, and slightly modified fluorinated versions of PiB, denoted Flutemetamol[85–87] and AZD4694,[88] have also been presented (Figure 2B). Overall, the chemical evolution of derivatives of CR and ThT has successfully generated ligands that can be used to image protein aggregates in diverse settings. Still, to assign and distinguish a variety of polymorphic shape-shifting protein aggregates, an arsenal of ligands is most likely required. In this regard, several molecular scaffolds have been presented as useful tools for detection of protein aggregates.[12,13,89–94] For some of these ligands, fluorescent assignment of different types of protein aggregates could be afforded due to the stabilization of the ground versus excited states of these ligands as a function of the polarity of their microenvironment.[91,92] Furthermore, a variety of near infrared emissive ligands optimized for optical *in vivo* imaging of protein aggregates has also been presented.[94–100] However, the focus of this review will be thiophene-based ligands, mainly luminescent conjugated oligo- and polythiophenes, that can be used for optical assignment of disease-associated protein aggregates.

3. Luminescent Conjugated Poly- and Oligothiophenes (LCPs and LCOs)

3.1. LCPs

Luminescent conjugated polythiophenes (LCPs) consist of several thiophene units with different side-chain functionalities along the conjugated thiophene backbone (Figure 3A). Due to their excellent photophysical properties, LCPs have been used as optical biosensors for a variety of biological processes, such as ligand-receptor interaction and DNA hybridization.[101–105] The

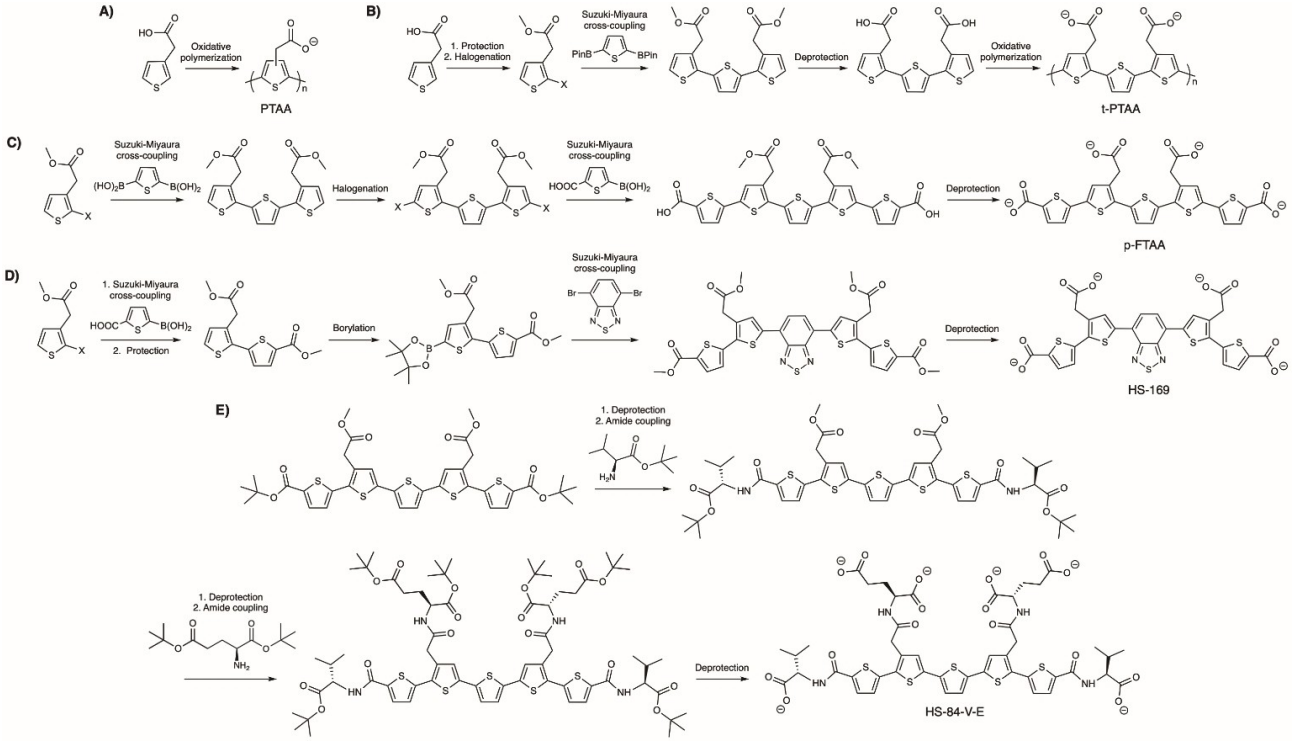

Figure 3. Chemical evolution of thiophene-based ligands. General synthetic routes for achieving the A) first and B) second generations of anionic luminescent conjugated polythiophenes (LCPs), PTAA (A) and t-PTAA (B). C) General synthetic route for achieving chemically defined luminescent conjugated oligothiophenes (LCOs) such as the anionic pentameric LCO p-FTAA. D) General synthetic route for achieving chemically defined donor-acceptor-donor (D–A–D)-based LCOs such as HS-169. E) General synthetic route for achieving chemically defined proteophenes with distinct amino acid side-chain functionalities along the thiophene backbone such as HS-84-V-E.

detection schemes of these sensors are employing the intrinsic conformation sensitive optical properties of the ligands since a conformational restriction of the flexible thiophene backbone will lead to a distinct optical fingerprint from the ligands. In 2003 and 2004,[106,107] Nilsson and co-workers showed that the spectral signature from zwitterionic and anionic LCPs could be used for the detection of conformational changes in synthetic peptides, and in the following year, the first study regarding LCPs as amyloid ligands was presented.[108] In this proof-of-concept paper, polythiophene acetic acid (PTAA) was used to detect amyloid fibril formation *in vitro* and later it was also shown that PTAA could be applied for histological staining of protein aggregates in tissue sections.[109] In addition, in contrast to conventional ligands, such as CR and ThT, PTAA has been used to distinguish different protein deposits due to changes in emission wavelengths when bound to different aggregated species.[110–112] This first generation of LCPs clearly showed promising qualities as amyloid imaging agents, but PTAA and other LCPs were afforded from oxidative polymerization of the respective thiophene monomers rendering a polydisperse material with a distribution of different thiophene chain lengths, as well as no regioregularity of the side-chain functionalities (Figure 3A). Furthermore, staining of protein aggregates could only be afforded under acidic or slightly alkaline conditions and some unspecific staining of other molecular entities in the tissue sections was also observed.[109–112]

To achieve slightly more chemically defined ligands, a second generation of LCPs based on oxidative polymerization of a trimer building block was generated.[113,114] The trimer building block was created by a palladium mediated Suzuki-Miyaura cross-coupling reaction of a mono-halogenated thiophene unit with a di-borylated thiophene (Figure 3B). Oxidative polymerization of these trimeric thiophenes rendered regioselective ligands, such as t-PTAA (Figure 3B), but a slight variation in chain length, 9 or 12 thiophene units, could still be observed.[113,114] From a biological perspective, the selectivity towards protein aggregates, both in solution and in tissue sections, was improved for the second generation of LCPs compared to the first generation, and optical separation of different protein aggregates could also be afforded with this generation of LCPs.[31,114] However, to use thiophene-based ligands under physiological conditions, as well as for live imaging of protein aggregates in vivo, further chemical improvement of this class of ligands was required.

3.2. LCOs

In 2009, Åslund and co-workers presented novel chemically defined anionic pentameric oligothiophenes that could be used

for two-photon imaging of protein aggregates in transgenic mice.[115] The design and synthesis were based on the previously described trimer building block[114] but instead of using oxidative polymerization, a halogenation of the trimer building block followed by palladium mediated Suzuki-Miyaura cross-coupling reaction of the trimer to borylated thiophene monomers was used (Figure 3C). These pentameric LCOs showed a great selectivity towards protein aggregates in tissue sections under physiological conditions, as well as a specific spectral signature upon binding to protein aggregates. In addition, protein aggregates comprised of the same protein could also be distinguished due to spectral alterations of the ligands, and after intravenous injection of the ligands in transgenic mice with aggregated Aβ pathology, the fluorescence from the ligands could be observed from protein aggregates in the brain by two-photon imaging through a cranial window.[115] Thus, the chemically improved pentameric LCOs showed enhanced selectivity towards protein aggregates compared to LCPs and could also be used for *in vivo* imaging. Later, several other chemically defined tetrameric, pentameric, hexameric and heptameric LCOs have been presented and these ligands have been generated by similar synthetic routes using palladium mediated Suzuki-Miyaura cross-coupling reactions of different halogenated or borylated thiophene building blocks.[115–122]

Due to their intrinsic fluorescence properties, LCOs offer the possibility to use a variety of imaging techniques, as well as different modes of detection, such as full excitation/emission spectra, and fluorescence decay time.[123] Nevertheless, the fluorescence characteristics of LCOs are to some extent restricted and thiophene-based ligands with extended photophysical properties are vital to design multiplex detection methodologies involving a combination of ligands or fluorophore-labelled antibodies towards distinct proteins. In this regard, donor–acceptor–donor (D–A–D)-based LCOs have been presented (Figure 3D).[124,125] These pentameric and heptameric D–A–D-based ligands were afforded by replacing the central thiophene unit with other heterocyclic moieties, such as benzothiadiazole (BTD) or quinoxaline, and in these ligands, the di- or tri-thiophene building blocks work as donors, whereas the BTD or quinoxaline moiety is the acceptor. The D–A–D-based ligands were assembled in palladium-mediated Suzuki–Miyaura cross-coupling reactions of different halogenated or borylated heterocyclic building blocks (Figure 3D). Like the LCOs, the D–A–D-based LCOs showed selectivity towards protein aggregates in tissue sections, but the D–A–D ligands displayed completely different excitation and emission characteristics, as well as different fluorescence decay times compared to the corresponding LCOs.[124–126] Thus, due to the design of D–A–D ligands, additional thiophene-based ligands with unique photophysical properties were afforded.

Recently, the chemical diversity of LCOs was enhanced even further as Björk and co-workers presented a novel class of pentameric LCOs, denoted proteophenes, with specific amino acid side-chain functionalization along the thiophene backbone (Figure 3E).[127] To generate ligands with homologous or heterologous amino acid side chain functionalities in the α- or β-positions along the pentameric thiophene backbone, a pentameric oligothiophene functionalized with methyl- and *tert*-butyl esters in orthogonal positions was synthesized. The pentameric proteophenes were achieved by palladium mediated Suzuki-Miyaura cross-coupling reaction of different thiophene building blocks followed by repetitive deprotecting reactions under either alkaline or acidic conditions, and hexafluorophosphate azabenzotriazole tetramethyl uronium (HATU)-mediated amide coupling reactions using different amino acids (Figure 3E). In addition, the concept of synthesizing D–A–D proteophenes with distinct photophysical properties was also shown.[127]

Overall, the chemical evolution of thiophene-based ligands from polydisperse LCPs to a diversity of chemically defined LCOs (Figures 3 and 4) has enhanced the toolbox of fluorescent ligands for optical assignment of disease-associated protein aggregates and in the next section, we will illustrate how both LCPs and LCOs have been applied to study these pathological entities in a variety of disease models as well as in patient derived tissue sections.

4. LCPs and LCOs for Optical Assignment of Disease Associated Protein Aggregates

4.1. LCPs

For more than a decade, LCPs and LCOs have been used for optical assignment of *in vitro* generated amyloid fibrils and protein aggregates in tissue sections, as well as for real-time *in vivo* imaging of protein deposits in cells and in animal models. In general, LCPs and LCOs have shown to identify a broader subset of protein aggregates than CR and ThT, as well as distinguish different types of aggregates that appear to be rather identical by CR, ThT or immuno-histological staining. The latter is achieved due to the unique conformational induced intrinsic photophysical properties of LCPs and LCOs, and this observation was first reported for protein deposits associated with distinct prion strains.[110] In brain tissue sections from transgenic mice inoculated with murine chronic wasting disease (mCWD) or natural scrapie (mSS), PTAA (Figure 3A) displayed different emission profiles when bound to the respective immuno-positive prion deposits (Figure 5). Thus, protein aggregates composed of the same protein could be distinguished due to alterations of the intrinsic fluorescence properties that were afforded from PTAA upon interaction with the respective protein aggregate. A similar variation in the PTAA emission profile was also obtained when staining prion fibrils that had been generated *in vitro* under different conditions, thus suggesting that the difference in PTAA emission was observed due to structural variations of the protein aggregates.[110] In the same study, it was also shown that PTAA identified prion aggregates that went undetected by both CR and ThT. Later, it was also shown that PTAA could be used for the spectral assignment of many other types of prion aggregates,[128–134] different Aβ aggregates in brain tissue sections from transgenic mice with AD pathology,[111] as well as protein deposits in tissue

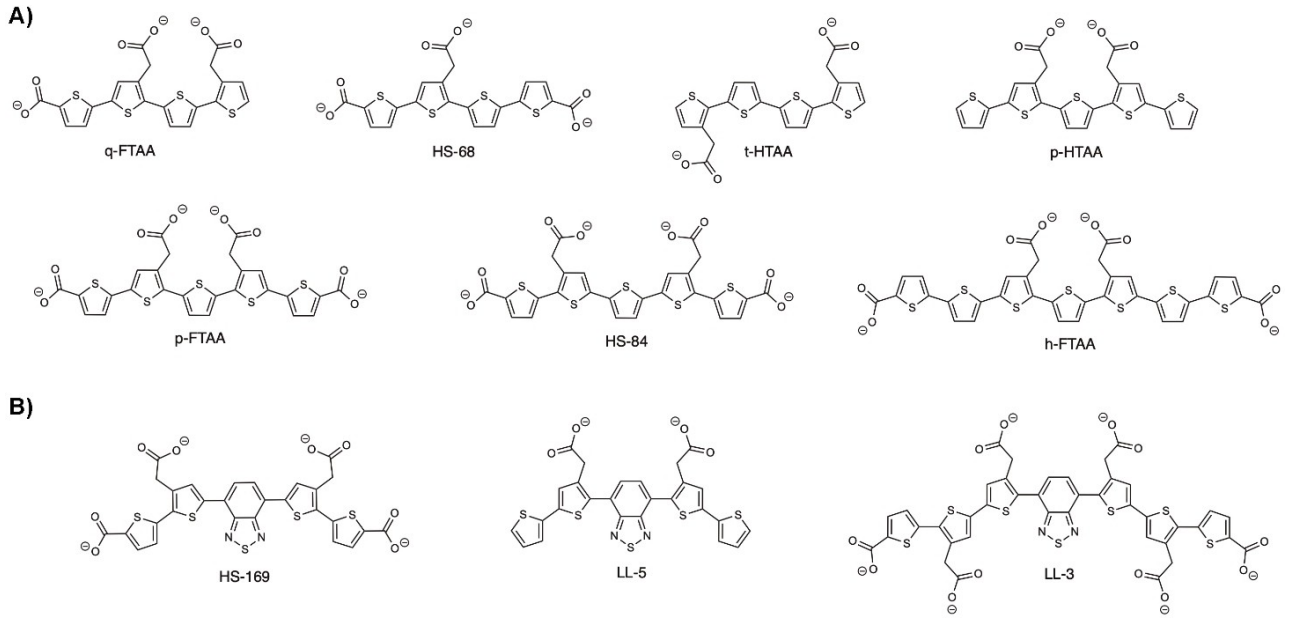

Figure 4. Examples of chemically defined LCOs that have been used for optical assignment of protein aggregates. A) Chemical structures of the anionic tetrameric LCOs, q-FTAA, HS-68 and t-HTAA, the anionic pentameric LCOs, p-HTAA, p-FTAA, and HS-84, as well as the anionic heptameric LCO, h-FTAA. B) Chemical structure of the D–A–D-based LCOs HS-169, LL-5 and LL-3.

sections from patients with different types of systemic amyloidosis.[112] In the latter study, PTAA was shown to emit different fluorescence when bound to the three most common systemic amyloids, AL, AA, and ATTR (Figure 5).[1] Hence, PTAA spectroscopy is a sensitive and powerful tool for identifying and characterizing protein deposits in systemic amyloidosis.

Similar to PTAA, the second generation of LCPs has also been used for spectral assignment of aggregated Aβ species in brain tissue sections from transgenic mice with AD pathology.[31,114] In the study by Heilbronner and co-workers,[31] the corresponding trimer based analogue to PTAA, t-PTAA (Figure 3B), was used to distinguish Aβ aggregates in mice intracerebrally injected with brain extract from different transgenic mouse models with aggregated Aβ pathology. Distinct spectral signatures were observed from t-PTAA stained Aβ deposits depending on the nature of the injected brain extract. Furthermore, the spectral signatures from the induced aggregates mimicked the emission profiles obtained from Aβ aggregates in the respective transgenic mouse model, indicating that the conformation of aggregated Aβ in transgenic mice can be maintained by seeded conversion.[31] Thus, the LCP spectral assignment of Aβ deposits assisted in revealing an underlying molecular mechanism for protein aggregation.

4.2. LCOs

4.2.1. Detection of non-thioflavinophilic and non-congophilic aggregates

The transformation of LCPs to chemically defined LCOs has, in addition to spectral assignment of protein aggregates, offered several novel possibilities to detect these pathological entities. In contrast to LCPs, chemically defined LCOs can be used to identify non-thioflavinophilic pre-fibrillar aggregates during the *in vitro* formation of amyloid like fibrils. This phenomenon was first reported[115,135] for the pentameric LCO denoted penta-formyl thiophene acetic acid (p-FTAA; Figure 4A), when using insulin or lysozyme, and later also for p-FTAA, as well as other anionic pentameric, hexameric and heptameric LCOs, when generating recombinant Aβ 1–42 amyloid like fibrils (Figure 6A).[117] p-FTAA has also been used for efficient imaging of non-thioflavinophilic protein aggregates in tissue samples from *Drosophila* models of human amyloidosis,[136–139] as well as for detection of intracellular protein aggregates, denoted protein inclusion bodies, in tissue samples from patients with sporadic inclusion body myositis (s-IBM) or chronic liver disorders (Figure 6B).[116,140] These protein inclusion bodies could also be observed with anionic heptameric LCOs and some of the ligands also revealed striking spectral differences between distinct protein inclusion bodies in s-IBM.[140] In addition, in liver tissue sections, LCOs were found to specifically bind to a distinct type of protein inclusion bodies known as Mallory-Denk bodies (MDBs), whereas a different type of hepatic protein inclusions, termed intracellular hyaline inclusions (IHBs), were negative for LCO staining.[116] Hence, LCOs could be used to discriminate between different inclusion bodies associated with different liver diseases. In a recent study, LCOs were also used to distinguish between intracellular filamentous inclusions of α-syn in PD and MSA.[141] An anionic tetrameric LCO, HS-68 (Figure 4A), revealed different emission profiles when bound to LBs and LNs in brain tissue sections from PD patients compared to GCIs in MSA (Figure 6C). Moreover, the anionic heptameric LCO, hepta-formyl thiophene acetic acid (h-FTAA; Figure 4A),

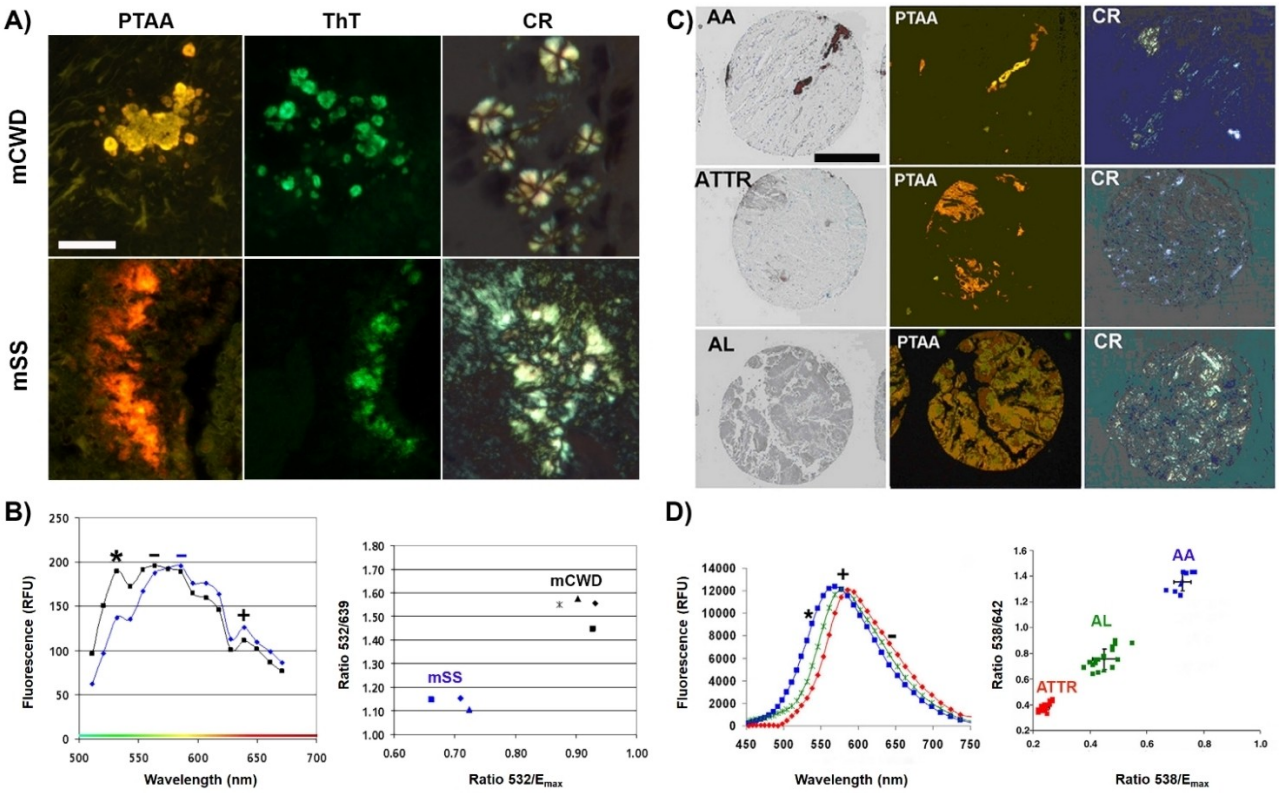

Figure 5. Spectral assignment of distinct protein aggregates with the anionic LCP PTAA. A) Images showing PTAA, ThT and CR bound to prion aggregates in brain tissue sections from transgenic mice inoculated with murine chronic wasting disease (mCWD) or natural scrapie (mSS). Scale bar: 50 μm. B) Spectra of PTAA (left) bound to mCWD (black) or mSS (blue) deposits. −: E_{max}, *: $E_{532\,nm}$, +: $E_{639\,nm}$. Correlation diagram (right) of the ratios of emitted intensities at the indicated wavelengths, $R_{532/639}$ and $R_{532/E_{max}}$, from PTAA bound to PrP plaques in individual mice inoculated with mCWD or mSS. C) Immuno-histochemical stains, CR polarization microscopy, and PTAA histochemistry of systemic amyloidosis. Top: Kidney sample of a patient diagnosed with AA amyloidosis. Middle: Heart sample of a patient diagnosed with ATTR amyloidosis. Bottom: Seminal vesicle sample of a patient diagnosed with AL amyloidosis. Scale bar: 250 μm. D) Left: Representative spectra from amyloid deposits stained with PTAA. For PTAA, spectra with emission maxima at 570 (blue), 580 (green), or 590 nm (red) were observed. The wavelengths used for calculation of the spectral ratios $R_{538/E_{max}}$ and $R_{538/642}$, 538 nm (*), E_{max} (+) and 642 nm (−), respectively, are highlighted. Right: Correlation diagram of the spectral ratios, $R_{538/Emax}$ and $R_{538/642}$, for PTAA when bound to amyloid deposits in tissue sections from different cases of systemic amyloidosis. The mean value of eight spots from 5 to 10 individual amyloid deposits in each tissue section is represented as a square. The samples segregated into three nonoverlapping groups. Comparisons with immuno-histochemical results revealed that these groups corresponded to AA, AL, and ATTR amyloidosis. Panels A, B adapted from ref. [110] with permission. Panels C, D adapted from ref. [112] with permission.

showed a clear difference in the distribution of fluorescence decay when interacting with the respective inclusion type.[141] Thus, LCO stained filamentous inclusions comprised of the same protein could be separated by hyperspectral microscopy or fluorescent lifetime imaging (FLIM).

4.2.2. Fluorescence lifetime imaging

FLIM is an exceedingly sensitive method, as it can monitor distinct rates of fluorescence decay after excitation and the decay rates do not depend on the concentration of the fluorophore.[142] Hence, FLIM is a direct approach for evaluating energy transfer between an excited molecule and its environment, and this technique has been extremely efficient in optical assignment of different prion aggregates in brain tissue sections.[123,143–145] In 2014, Magnusson and co-workers[123] showed that prion aggregates associated with the previously reported[98] mouse adapted prion strains, mCWD and mSS, could be distinguished by FLIM after being stained with anionic pentameric or heptameric LCOs. The most efficient separation of the prion deposits was achieved by h-FTAA (Figure 4A) staining, which resulted in a complete separation of the fluorescence decays from the strain-specific deposits (Figure 7A).[123] Differences in the distribution of fluorescence decay from h-FTAA bound to prion deposits have later been used to show that polymorphic prion deposits is involved in several biological processes.[143–145] Furthermore, FLIM has also been used to assign distinct h-FTAA stained aggregated Aβ morphotypes in transgenic mouse models.[146] Thus, the alterations of the fluorescence decays from an LCO bound to protein aggregates have enabled the possibility of assigning distinct protein deposits and to pinpoint their potential role in the pathogenesis of the disease. Lately, the LCO-FLIM methodology has been evolved further by using combinations of LCOs and D–A–D-based LCOs.[127,147] As D–A–D ligands display completely different fluorescence decay times compared to pure thiophene-based LCOs,[126] combinations of ligands can be

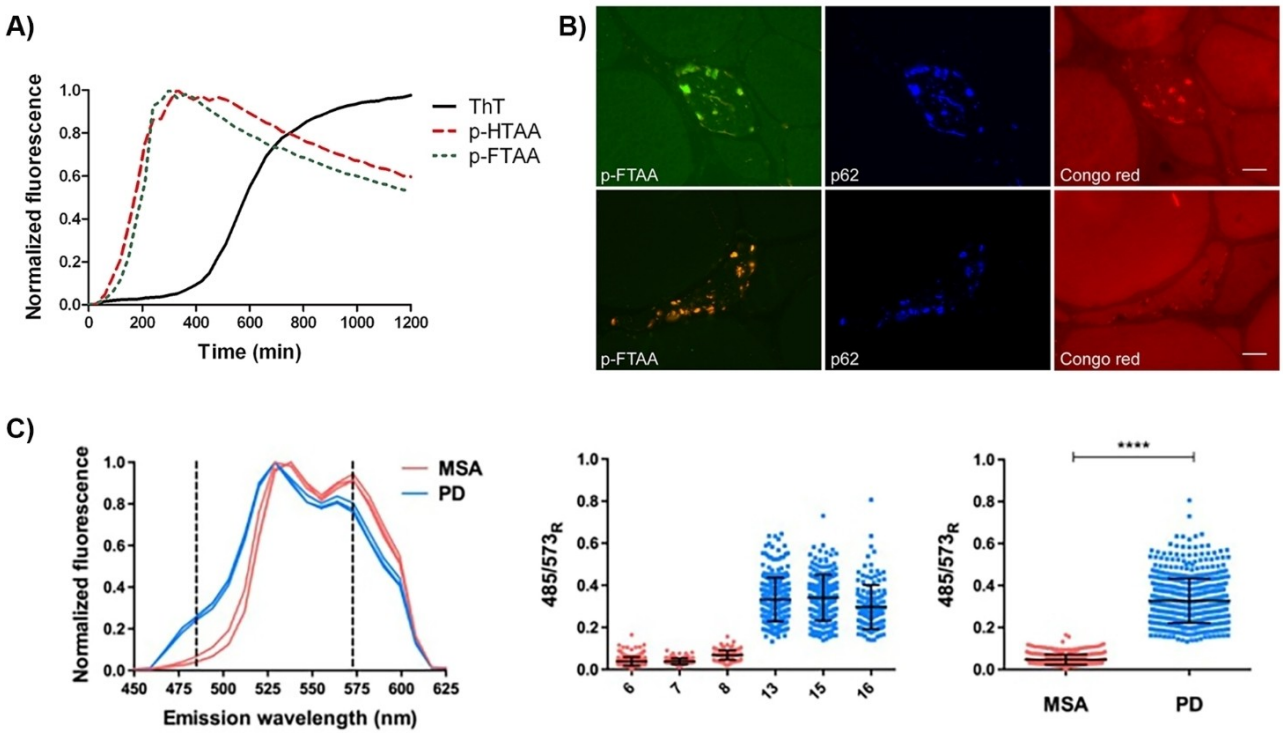

Figure 6. Detection of non-thioflavinophilic and non-congophilic aggregates with LCOs. A) Time plot showing the fibril formation kinetics of Aβ1–42 monitored by fluorescence from ThT or the LCOs p-HTAA and p-FTAA. The pentameric LCOs detect early non-thioflavinophilic species in the fibril formation pathway and showed initiation of a growth phase after only 60 min. B) Fluorescence images of consecutive muscle sections from s-IBM patient double-stained with p-FTAA and p62 antibody (left and middle) or singly stained with Congo Red (right). Scale bars: 20 μm. C) Spectral analysis of HS-68 and pS129 α-syn antibody-positive inclusions in multiple system atrophy (MSA) and Parkinson's disease (PD). Left: Mean emission spectra of HS-68 binding to pS129 α-syn positive deposits in three MSA cases and three PD cases. Middle: Plot of the ratio of emission intensity at wavelengths 485 and 573 nm for HS-68 when binding to inclusions in MSA (red circles) and PD (blue squares) that were also labelled with pS129 α-syn antibody. Right: Merging of the ratio values for all MSA and PD cases shown in the middle panel. The results are expressed as means ± S.D. ($n = 3$) **** $p < 0.0001$. Panel A reproduced from ref. [117] with permission from the Royal Society of Chemistry. Panel B reproduced from ref. [140] with permission. Panel C reproduced from ref. [141] with permission through Creative Commons Attribution 4.0 International License (http://creativecommons.org/licenses/by/4.0/). Copyright: 2019, The Authors.

applied for histological staining of tissue sections. Such a dual staining protocol, allowing multiplex photophysical detection of distinct protein aggregates in brain tissue sections with AD pathology, was afforded when combining two proteophenes, HS-84-V-E (Figure 3E) and HS-169-V-V, with distinct amino acid side-chain functionalities along the conjugated thiophene backbone.[127] As the selectivity of the proteophenes towards AD associated pathological hallmarks was highly dependent on the chemical nature, as well as on the location of the amino acid functionality, a differential staining of Aβ or tau aggregates was observed. Characteristic lifetime distributions (600 and 1000 ps) from HS-84-V-E were observed from Aβ cored plaques, diffuse Aβ plaques, cerebral amyloid angiopathy (CAA) lesions and tau pathology, whereas longer decay times, 2000–3000 ps, associated with HS-169-V-V could only be detected from CAA lesions (Figure 7B).[127] Thus, due to differential binding modes of proteophenes with distinct photophysical properties, assignment of different aggregated pathologies in human AD brain tissue sections could be afforded by FLIM.

4.2.3. Hyperspectral imaging with a single LCO

Similar to LCPs, a variation of chemically defined LCOs has also been applied for hyperspectral assignment of distinct protein aggregates in tissue sections.[112,115,117,118,121,125,140,141,148–160] This proof of concept was first shown for the anionic pentameric LCO p-FTAA (Figure 4A), since this ligand could be utilized to distinguish protein aggregates associated with prion strains.[115] In a similar fashion as the LCP PTAA,[110] different emission signatures were afforded from p-FTAA when bound to prion deposits from two mouse adapted prion strains (Figure 8A). Furthermore, p-FTAA demonstrated different emission profiles when bound to Aβ compared to tau aggregates in brain tissue sections with AD pathology, whereas PTAA showed similar spectral profiles from these pathological entities (Figure 8B).[115] Thus, spectral assignment of the two pathological hallmarks in AD, assemblies of Aβ or tau, could only be obtained by the chemically defined LCO p-FTAA, signifying that novel possibilities for optical assignment of protein aggregates were afforded with chemically defined ligands. Later on, fluorescence signatures from p-FTAA have also been used to assign distinct protein deposits in tissue sections from systemic amyloidosis[112]

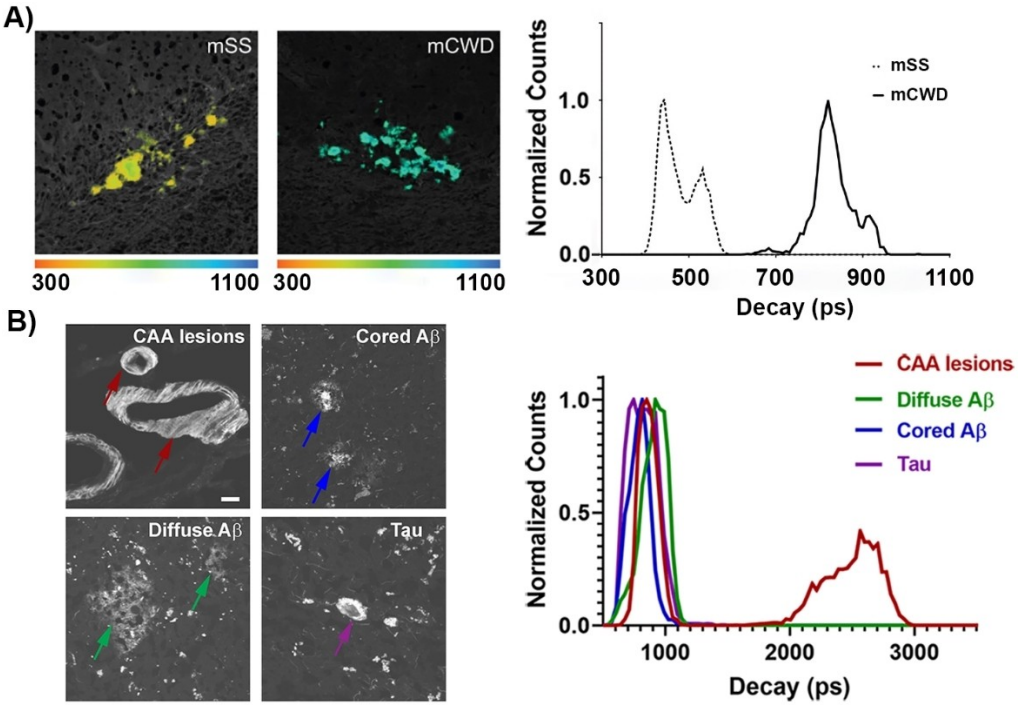

Figure 7. Detection of different protein aggregates by FLIM. A) Left: Fluorescence lifetime images of h-FTAA bound to prion deposits in brain tissue sections from mice inoculated with mCWD or mSS. Right: Lifetime decay curves of h-FTAA bound to mCWD or mSS deposits. The colour bars represent lifetimes from 300 (orange) to 1100 ps (blue), and the images are colour coded according to the representative lifetime. The fluorescence lifetimes were collected after excitation at 490 nm. B) Intensity images (left) and fluorescence lifetime distributions (right) from CAA lesions (red arrows), cored Aβ plaques (blue arrows), diffuse Aβ plaques (green arrows) or tau pathology (purple arrow) in a human AD brain tissue section stained with 100 nM HS-169-V-V and 100 nM HS-84-V-E. The fluorescence lifetime distributions were recorded by using excitation at 490/565 nm. Scale bar: 20 μm. Panel A adapted from ref. [123] with permission through Creative Commons Attribution-Non-Commercial License (http://creativecommons.org/licenses/by-nc/3.0/). Copyright: 2014, The Authors. Panel B reproduced from ref. [127] with permission.

and in transgenic mouse models with aggregated Aβ,[148–153] α-syn[154] or prion pathology.[155] Hence, p-FTAA has been used for spectral assignment of a diversity of protein aggregates in patient derived tissues, as well as brain tissue sections from transgenic mouse models for proteopathic NDs.

In addition to p-FTAA, the tetrameric LCO HS-68 (Figure 4A) has been used for efficient spectral assignment of distinct protein aggregates in tissue sections. HS-68 was first presented by Klingstedt and co-workers in 2013,[118] and in this study, it was shown that the ligand could be employed for spectral assignment of Aβ and tau deposits in human brain tissue sections with AD pathology. In a follow up paper, HS-68 also showed spectral differentiation assigned to age-dependent polymorphism of Aβ and tau aggregates in transgenic mouse models (Figure 8C).[121] In young APPPS1 transgenic mice, the core of the Aβ plaques showed yellow HS-68 fluorescence, while red fluorescence was seen from the rim surrounding the centre of the plaques. In older mice, HS-68 fluorescence was blue-shifted when bound to both the core and the more diffuse structure around the plaques which resulted in green-coloured deposits (Figure 8C).[121] In young P301S tau transgenic mice, HS-68 showed yellow-red fluorescence from loosely packed tau assemblies that often appeared granular, whereas tau inclusions in older mice were of a different type. These assemblies displayed a more dense and homogenous morphology, and the emission of HS-68 was blue-shifted upon binding.[121] Hence, the emission properties of HS-68 when bound to Aβ or tau deposits could be linked to a distinct age of the mice. This phenomenon was more evident for tau, as two different types of aggregates could be found in young and old P301S tau mice, respectively.[121] The more dense, homogenous aggregates with a blue-shifted HS-68 emission spectrum appeared in mice at four months of age, while the granular-like assemblies with a more red-shifted HS-68 spectrum were found already in one-month-old mice. A connection between the dense aggregates in older mice and neurodegeneration was also suggested as severe disease symptoms occurred in mice that were five to six months old.[121] As mentioned in a previous section, a similar spectral variation of HS-68 has also been observed when the ligand was binding to assemblies of α-syn in PD and MSA.[141] In the analysis, LBs and LNs in PD brain tissue samples displayed a blue-shift of HS-68 emission compared to GCIs in MSA, suggesting that inclusions in PD are more mature.[141]

Besides the FLIM applications described earlier, the heptameric LCO h-FTAA (Figure 4A) has also been used for hyperspectral assignment of protein aggregates in tissue sections. Similar to the two other LCOs, p-FTAA and HS-68, h-FTAA has been applied for spectral assignment of different aggregated Aβ species in transgenic mouse models,[156] as well as Aβ and tau deposits in human brain tissue sections from patients

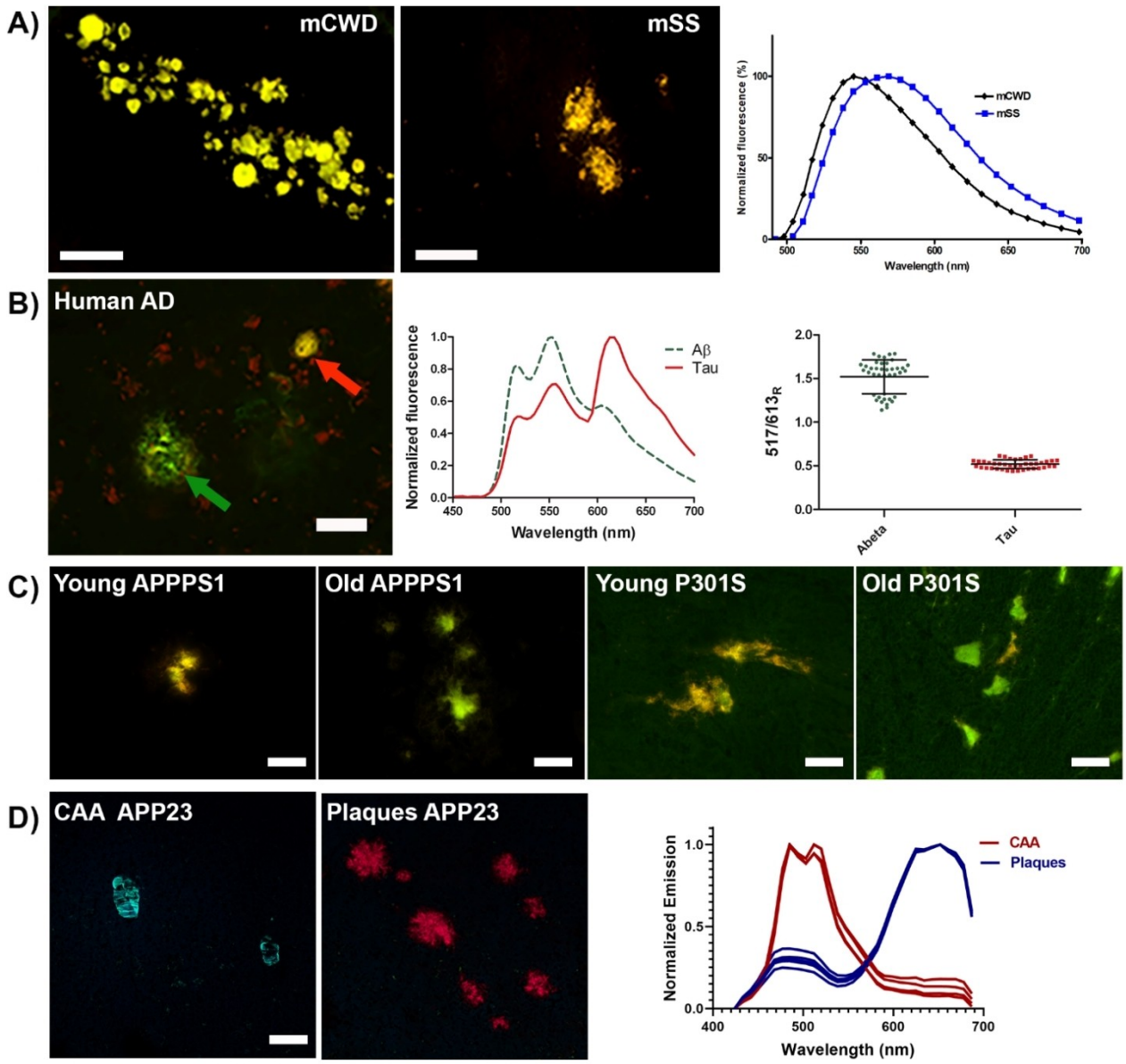

Figure 8. Hyperspectral imaging of protein aggregates with a single LCO. A) *Ex vivo* fluorescence images of p-FTAA-labelled prion deposits in mice infected with mouse-adapted chronic wasting disease, mCWD (left) or mouse-adapted sheep scrapie, mSS (middle) that have been intracerebrally injected with p-FTAA; scale bars: 50 μm. Typical p-FTAA emission spectra (right) when bound to mCWD or mSS deposits. B) Left: Fluorescence image of p-FTAA bound to Aβ plaque (green arrow) and a tau neurofibrillary tangle (red arrow) in AD human brain tissue sections. Middle: merged emission spectra from p-FTAA bound to Aβ or tau deposits after using excitation at 405 and 546 nm; scale bar: 20 μm. Right: Plot of the ratio of light intensity emitted at 517 and 613 nm ($517/613_R$) for p-FTAA, bound to Aβ plaques or tau NFTs shown with standard deviation. The intensities were obtained from the double-excitation spectra.
C) Fluorescence images of Aβ deposits in frozen brain sections from young or old APPPS1 transgenic mice (left) and of tau deposits in frozen brain sections from young or old P301S tau transgenic mice (right) labelled with HS-68; scale bars: 20 μm. D) Fluorescence images of LL-3-labelled CAA (left) and Aβ plaques (middle), as well as emission spectra (right) for the ligand bound to the different Aβ deposits in brain tissue sections from in APP23 transgenic mice upon excitation at 405 nm. Spectra were collected from 10 individual deposits; scale bar: 50 μm. Panel B adapted from ref. [117] with permission from Royal Society of Chemistry. Panel C adapted from ref. [121] with permission. Panel D adapted from ref. [125] with permission.

diagnosed with AD.[117] In addition, h-FTAA has been proven to be very efficient in detecting protein aggregates in subcutaneous fat tissue or tissue sections from patients with systemic amyloidosis.[157–160] In these studies, h-FTAA was benchmarked towards CR and it was shown that h-FTAA was a sensitive, rapid and powerful tool for identifying protein deposits in tissue sections, as well as in fat biopsies. Thus, h-FTAA staining might be employed as a complementary technique for accurate detection of amyloid deposits in routine pathology settings and serve as a diagnostic tool for systemic amyloidosis.

The latest generations of LCOs, D–A–D-based LCOs and proteophenes have also been used for spectral assignment of different protein aggregates. In a study by Shahnawaz and co-workers, the pentameric D–A–D-based LCO, HS-169 (Figure 4B), displayed different spectral signatures when bound to amplified α-syn aggregates derived from patients with PD or MSA.[161] In

addition, a heptameric D–A–D-based LCO, LL-3 (Figure 4B), showed two distinct emission profiles when bound to CAA or Aβ cored plaques in brain tissue sections from a transgenic mouse model with Aβ pathology (Figure 8D).[125] Thus, the spectral signatures from LL-3 could be used to distinguish these two aggregated Aβ species and these spectral signatures were presumably obtained due to different binding modes of LL-3 to CAA or Aβ plaques. As mentioned above, differential binding modes to different aggregated Aβ species, as well as tau pathology, in human AD brain tissue sections were also observed for proteophenes with distinct amino acid side-chain functionalities,[127] thus signifying that ligands with different binding modes to distinct aggregated pathologies can be utilized for spectral assignment of protein aggregates in tissue sections.

4.2.4. Hyperspectral imaging with combinations of LCOs

In addition to staining procedures including a single LCO, protocols with combinations of different LCOs have been used for optical assignment of protein aggregates. The first dual staining protocol was reported by Nyström and co-workers in 2013,[32] and in this study, a combination of the tetrameric LCO, quadro-formyl thiophene acetic acid (q-FTAA) (Figure 4A), and the heptameric LCO, h-FTAA (Figure 4A), was used to show an age-dependent *in vivo* conformational rearrangement of Aβ deposits in different transgenic mouse models with AD pathology. These two LCOs, q-FTAA and h-FTAA, have slightly different fluorescence profiles and by calculating the ratio of the intensity of the emitted light correlated to each LCO, it was shown that h-FTAA emission was dominating for deposits found in young mice, whereas in older mice, q-FTAA fluorescence was more prominent in the cores of the plaques, while the peripheral plaque coronas still showed fluorescence from h-FTAA (Figure 9).[32] As described above, this age-related alteration of Aβ deposits was later confirmed with HS-68,[121] and from a biological perspective, the dual staining protocol with q-FTAA and h-FTAA has also been applied for showing seed-dependent templating of murine AA amyloidosis,[162] Aβ polymorphisms in different etiological subtypes of AD (Figure 9C),[33,163] different cellular Aβ aggregates in Drosophila,[164] as well as different biochemical alterations associated with Aβ polymorphism in AD.[165,166] In the latter studies,[164–166] the LCO double staining was performed together with imaging mass spectrometry (IMS), and by combining these techniques, a correlation between the LCO spectral signatures and the biochemical composition of different Aβ deposits could be afforded. Moreover, in an *in vitro* study of Aβ1-40 fibril formation, the results suggested that differences in q-FTAA versus h-FTAA binding were correlated with fibrils transforming from solitary filaments into higher order bundled structures.[167] Recently, the q-FTAA and h-FTAA dual staining protocol was applied for whole-brain microscopy imaging of clarified brains from transgenic mice with aggregated Aβ pathology, and the optical signatures from the LCOs assisted in revealing difference in temporal and spatial efficacy of anti-Aβ therapies.[168]

Lately, dual staining protocols with combinations of pure thiophene based LCOs and D–A–D-based LCOs were presented.[147] In the study by Lantz and co-workers, the pentameric ligands LL-5 (Figure 4B) and p-FTAA (Figure 4A) were used for spectral assignment of different aggregated Aβ species and tau pathologies in human AD brain tissue sections (Figure 9D). In comparison to q-FTAA and h-FTAA, these ligands showed less spectral overlap as p-FTAA emission maxima are observed at 515 and 545 nm, whereas LL-5 displays an emission maximum at 625 nm (Figure 9E). Furthermore, these ligands also displayed completely different distribution of decays, 600 to 1200 ps for p-FTAA and 2000 to 3500 ps for LL-5, allowing assignment of different protein deposits with FLIM (Figure 9E). Likewise, another combination of a tetrameric LCO, t-HTAA (Figure 4A), and a D–A–D based LCO, HS-169 (Figure 4B), could also be applied for optical assignment of distinct protein aggregates with FLIM (Figure 9F and G). The characteristic decays around 4000 ps from HS-169, could be observed from both CAA and diffuse Aβ plaques, whereas the shorter decays, around 500 ps, from t-HTAA were only obtained from CAA. Thus, this combination of ligands could be used to distinguish different aggregated Aβ species in human AD brain tissue sections. Overall, the next generation of dual staining protocols comprised of thiophene-based ligands with distinct photophysical properties, as well as differential binding modes to specific protein aggregates, might offer the possibility to resolve aggregate polymorphism in a more refined manner.

4.2.5. In vivo imaging

In contrast to LCPs, the chemically defined LCOs showed specific staining of protein aggregates in tissue sections under physiological conditions (phosphate buffered saline pH 7.4).[115,117] Thus, it should be possible to utilize the LCOs for real-time *in vivo* optical imaging of protein deposits in cells and animal models. As mentioned above, the proof-of-concept for *in vivo* imaging of protein aggregates was first shown for a set of anionic pentameric oligothiophenes, including p-HTAA and p-FTAA (Figure 4A).[115] After an intravenous injection of p-HTAA in the tail vein of transgenic mice, the characteristic spectral signature from the LCO could be afforded from Aβ aggregates in the brain by multiphoton imaging through a cranial window (Figure 10A). Hence, p-HTAA, as well as p-FTAA, crossed the blood–brain barrier, and the ligand could be used for optical imaging of Aβ deposits in the brain of sedated transgenic mice with Aβ pathology. Moreover, *ex vivo* analysis of brain tissue sections from prion infected mice injected with p-FTAA showed that prion aggregates associated with distinct prion strains were labelled with the ligand and displayed different p-FTAA emission spectrum (Figure 8A).[115] Later on, it was also shown that intravenously injected p-FTAA was binding to tau deposits in the brain of P301S tau transgenic mice, and in the same study, p-FTAA was also used for real-time identification of filamentous tau aggregates in dorsal root ganglion neurons cultured from adult P301S tau mice.[169] The heptameric LCO, h-FTAA, has also been shown to pass the blood-brain barrier after

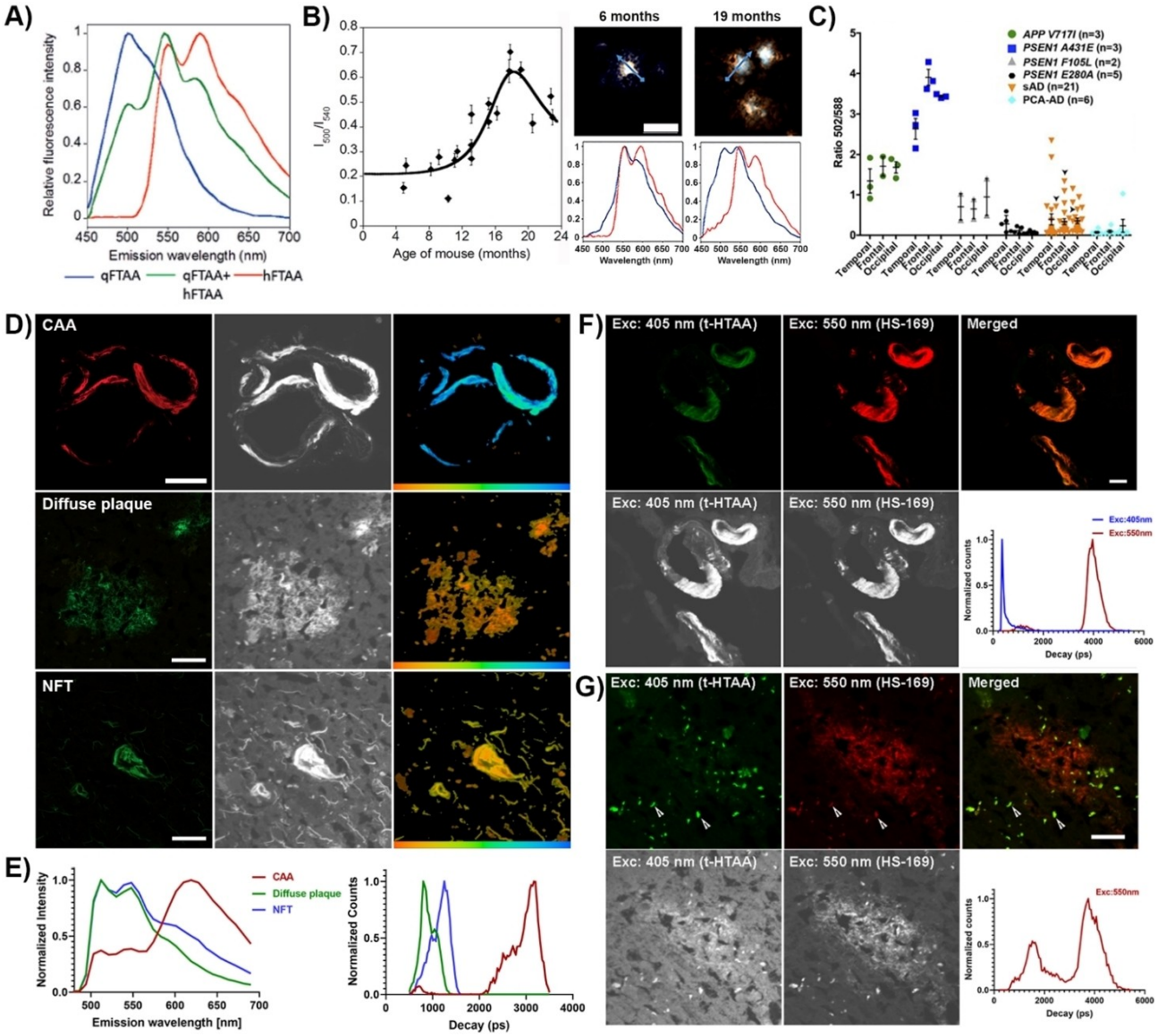

Figure 9. Hyperspectral imaging of protein aggregates with a combination of LCOs. A) Normalized emission spectra from q-FTAA or h-FTAA when labelling Aβ plaques in brain tissue sections. The mathematical sum of the two separate spectra is shown in green. B) Diagram showing the ratio of intensity of the emitted light at 500 and 540 nm, I_{500}/I_{540}, from Aβ plaques in brain tissue sections from APPPS1 mice stained with q-FTAA and h-FTAA versus the age of the mice (left). The fluorescence intensity at 500 nm (I_{500}) reflects q-FTAA emission, whereas the intensity at 540 nm (I_{540}) reflects h-FTAA emission. The diagram reveals an age-dependent variation of plaque staining in APP/PS1 mice when stained simultaneously with q-FTAA and h-FTAA. Images of individual plaques in 6- or 19-month-old APP/PS1 mice (right). Normalized spectra from the central part (blue) and periphery (red) of the plaques are displayed below each image; scale bar: 50 μm. C) Diagram showing the ratio of fluorescence intensity at 502 and 588 nm; this represents the fluorescence emission peaks of q-FTAA and h-FTAA, respectively, from Aβ plaques in different brain regions from familial AD (*APP V717I, PSEN1A431E, PSEN1 F105L, and PSEN1 E280A*), typical sporadic AD (sAD), and sporadic posterior cortical atrophy (PCA)-AD cases. Error bars represent the SEM. D) Fluorescence assignment of protein aggregates in brain tissue sections with AD pathology stained with a combination of p-FTAA and LL-5. Spectral (left), FLIM (middle) and colour coded FLIM (right) images from different aggregated Aβ pathologies, CAA and diffuse plaque, and tau pathology (NFT) with excitation at 490 nm. The colour bars (right) represent 500 (red) to 3500 ps (blue); scale bars: 50 (CAA) and 20 μm (diffuse plaque and NFT). E) Left: Emission spectra from different aggregated Aβ (CAA and diffuse plaque) and tau (NFT) with excitation at 490 nm. The p-FTAA emission maxima are observed at 515 and 545 nm, whereas LL-5 displays an emission maximum at 625 nm. Right: Fluorescent decays from different aggregated Aβ (CAA and diffuse plaque) and tau pathologies (NFT) with excitation at 490 nm. The distribution of decays for p-FTAA is observed between 600 and 1200 ps, whereas LL-5 displays distributions of decays between 2000 and 3500 ps. F), G) Fluorescence assignment of protein aggregates in brain tissue sections with AD pathology stained with a combination of t-HTAA and HS-169. Colour-coded fluorescence images (top), FLIM intensity images and fluorescence decays (bottom) of F) CAA and G) diffuse Aβ plaques. For t-HTAA, excitation at 405 nm was used and emission was recorded from 470 to 545 nm, whereas HS-169 was excited at 550 nm and emission was detected between 610 and 745 nm. Autofluorescence from lipofuscin is highlighted with white arrow heads; scale bars: 20 μm. Panels A, B adapted with permission from ref. [32]. Copyright: 2013, American Chemical Society. Panel C adapted from ref. [33] with permission. Panels D-G adapted from ref. [147] with permission.

intravenous administration in transgenic mouse models with Aβ or tau pathology. The ligand revealed a distinct shift in its emission spectrum when it was binding to Aβ plaques versus tau lesions, as well as Aβ plaques versus CAA.[170] Thus, in

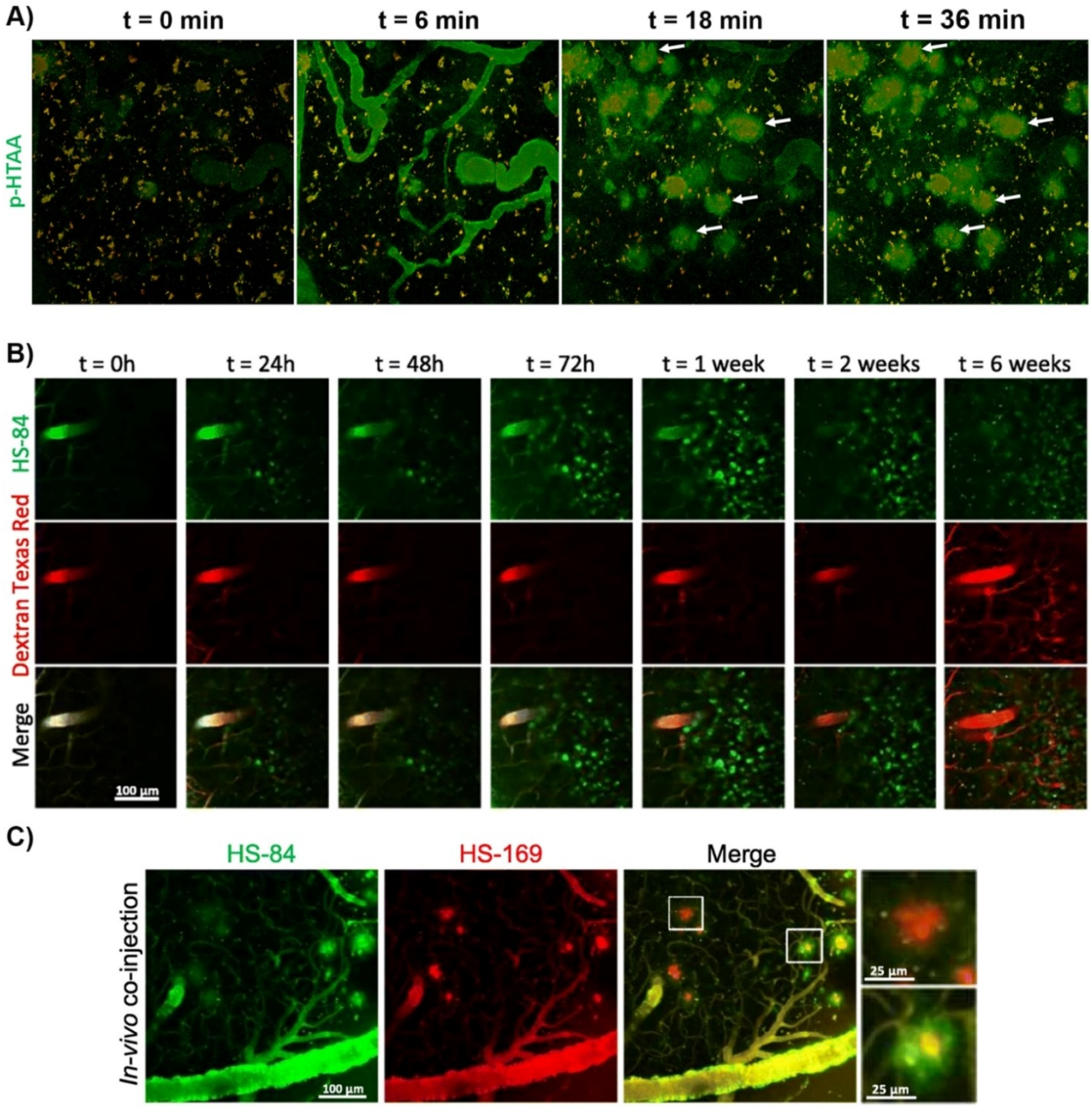

Figure 10. Optical *in vivo* imaging of protein aggregates with LCOs. A) Real-time in-vivo multiphoton imaging of Aβ deposits in the brain through a cranial window after an intravenous injection with p-HTAA in the tail vein of a 10-month-old APPPS1 mouse. p-HTAA fluorescence (green) is first observed in the cerebral blood vessels with subsequent diffusion into the brain parenchyma. Within minutes, labelling of cerebral plaques is observed, and after longer incubation periods, intense p-HTAA fluorescence is only seen from cerebral plaques. Representative LCO-labelled plaques are indicated by white arrows. B) Images showing different time points after intravenous injection of HS-84 in rTg4510 tau transgenic mice with aggregated tau pathology. $t = 0$ represents imaging a few minutes after injection. Dextran Texas Red was systematically injected to create a fluorescent angiogram. Multiphoton imaging was performed through a cranial window. Scale bar: 100 µm and applies to all images. C) Representative *in vivo* multiphoton microscopy images of HS-84 and HS-169 in the same brain area in an APPPS1 transgenic mouse with aggregated Aβ pathology. Note heterogeneity among plaques. A mouse carrying a cranial window was simultaneously injected with HS-169 and HS-84 and subjected to multiphoton microscopy 24 h later. Panel A reprinted with permission from ref. [115]. Copyright: 2009, American Chemical Society. Panels B, C reproduced from ref. [172] with permission through Creative Commons Attribution 4.0 International License (http://creativecommons.org/licenses/by/4.0/). Copyright: 2019, The Author(s).

contrast to other ligands, such as Methoxy-X-04,[75] which has been applied for *in vivo* two-photon imaging of protein deposits, h-FTAA allowed *in vivo* differentiation of distinct protein aggregates. In a more recent study, h-FTAA was applied, together with large-field multifocal illumination (LMI) fluorescence microscopy, to perform a transcranial detection of tauopathy over the entire cortex of P301L mice.[171]

In addition to p-HTAA, p-FTAA and h-FTAA, the pentameric D–A–D-based LCO, HS-169 (Figure 4B), has also been utilized for real time *in vivo* imaging of protein aggregates in animal

models.[172,173] In a study by Calvo-Rodriguez and co-workers,[172] individual tau or Aβ deposits in transgenic mouse models were labelled *in vivo* with HS-169, as well as the corresponding pentameric LCO, HS-84 (Figure 4A), and imaged over time with multiphoton microscopy. After a single intravenous injection of the ligands, HS-84 allowed longitudinal imaging of tau tangle dynamics, whereas HS-169 could be used to visualize Aβ deposits (Figure 10B).[172] The longitudinal imaging after a single injection was afforded since the ligands remained in the circulation for several days. In addition, co-injection of HS-84 and HS-169 could also be used for discriminating Aβ aggregate subtypes, since HS-169 labelled aggregates emitted light with a different wavelength compared to HS-84 stained deposits (Figure 10C).[172] Thus, similar to the observations reported earlier for histological staining of tissue sections,[127,147] a combination of a pure thiophene-based LCO and a D–A–D-based LCO could be used for spectral assignment of protein deposits comprised of the same protein in the brain of a living mouse. Later, HS-169 was also used for multiscale optical and optoacoustic imaging of Aβ aggregates in mice.[173]

Overall, the optical assignment of protein aggregates using LCOs in tissue sections from transgenic mouse models or patients, as well as living cells and animals, has been very successful and generated several molecular insights regarding protein aggregate polymorphism and the potential role of distinct protein deposits in the pathogenesis of the disease. In addition, when applied for live-imaging of protein aggregates in cells or in transgenic animals,[115,169–173] the LCOs have not displayed any severe cellular or acute toxicity, as well as been shown to readily enter cells and label intracellular protein aggregates. Therefore, it would be very interesting to convert the LCOs into agents, such as PET tracers, that can be utilized for clinical imaging. As shown by Nordeman and co-workers, when converting q-FTAA and p-FTAA to 11 C or 18F labelled PET tracers (Figure 11), specific binding to amyloid deposits was found in the heart, kidney, liver, and spleen.[174] Furthermore, combined PET and computer tomography (CT) experiments in a healthy monkey showed very low uptake in the brain, pancreas, and heart of the healthy animal, suggesting low nonspecific binding to normal tissue. Thus, the study indicated that radiolabelled LCOs might be used as tracers for the visualization of amyloid deposits in various organs in systemic and localized amyloidosis. However, although these ligands displayed high selectivity and affinity towards these pathological entities, the pharmacokinetic properties of the LCOs might be suboptimal for PET imaging, especially in the brain. For longitudinal multiphoton imaging, it was advantageous that the ligands remained in the circulation for several days after a single injection.[172] However, for optimal PET tracers, a rapid clearance is preferable.[80] In addition, the blood-brain barrier passage of properly functionalized LCOs is most likely due to an active transport. An analogue to p-FTAA with methyl esters instead of free carboxyl groups in the β-position, could be used for histological staining of protein aggregates, but when this ligand was used for *in vivo* imaging through a cranial window, staining of aggregates in the brain was lacking.[115] Thus, free carboxyl groups in the β-position is presumably a crucial chemical determinant for the LCOs to pass the blood-brain barrier, and if it is an active transport, higher concentrations than normally used for PET tracers are likely necessary to get the LCOs into the brain. Overall, further chemical improvements are necessary to achieve LCO-based ligands for clinical imaging. Nevertheless, LCOs have shown to be efficient ligands for optical imaging of protein aggregates and in the next section, we will discuss the binding modes of LCOs to protein deposits, as well chemical determinants that have shown to be crucial to achieve superior ligands for optical assignment of disease-associated protein aggregates.

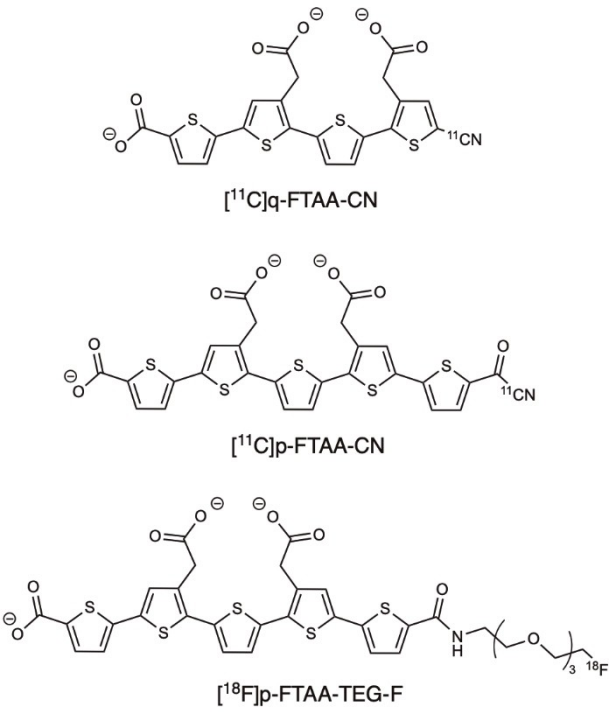

Figure 11. Chemical structure of LCO based PET tracers: the tetrameric LCO, [11C]q-FTAA-CN (top), as well as the pentameric LCOs [11C]p-FTAA-CN (middle) and [18F]p-FTAA-TEG-F (bottom).

5. LCOs: Binding Modes and Chemical Determinants for Superior Ligands

Due to the evolution of chemically defined LCOs, it has been possible to obtain plausible binding modes to protein aggregates for these ligands.[122,175,176] In addition, due to minor chemical variations of the ligands, chemical determinants for achieving superior ligands for optical separation of distinct protein aggregates have been identified.[115,117,118,120,121,125,127] In 2015, Hermann and co-workers showed that p-FTAA (Figure 4A) binds to amyloid fibrils in a similar way as the conventional ligand CR.[122] By using the prion-forming domain of the fungal HET-s prion as a model, solid-state nuclear magnetic resonance analyses and molecular dynamics simulations showed that

anionic side chains of p-FTAA interacted with complementary, regularly spaced lysine residues situated in well-accessible grooves along the HET-s fibrils (Figure 12A).[122] Later, similar binding modes to HET-s fibrils were also observed for heptameric LCOs, as well as for the LCP PTAA, and the interaction with regularly spaced surface charge patterns and well-accessible grooves on the fibril could also be assigned to distinct fluorescence wavelengths of the ligands.[175] A correlation between binding mode and optical properties has also been shown for p-FTAA bound to Aβ 1–42 fibrils.[176] An extremely stable binding site for the interaction between p-FTAA and Aβ 1–42 fibrils was identified by molecular dynamics simulations and when bound to the fibrils, p-FTAA was locked in an all-trans conformation due to interactions between the anionic carboxyl groups and the cationic lysine side chains. Hence, upon binding, p-FTAA showed a pronounced increase in molecular planarity and this conformational change is in line with the observed changes in photophysical properties of the ligand bound to protein aggregates.[115,117,177,178] A study by Bäck and co-workers has also confirmed the CR-like binding mode of LCOs to Aβ aggregates, since anionic oligothiophenes were shown to efficiently displace X-34, a CR analogue, but not PiB from recombinant Aβ amyloid fibrils and AD brain-derived Aβ (Figure 12B).[179] When comparing q-FTAA, p-FTAA and h-FTAA (Figure 4) towards AD brain-derived Aβ aggregates, p-FTAA showed the lowest EC_{50} value, 0.7 nM, whereas q-FTAA showed the highest value (300–500 nM). However, when replacing the α-terminal hydrogen with other groups, the binding of the tetramer q-FTAA was improved. The lowest EC_{50} value, <0.1 nM, was achieved for q-FTAA-CN, which has an α-terminal nitrile group (Figure 12C). Thus, minor chemical alterations of the moiety in the α-terminal position highly influenced the binding mode of tetrameric LCOs to aggregated Aβ species derived from human AD brain, and when 100 nM q-FTAA-CN was used for histological staining of human AD brain tissue sections, selectivity towards aggregated Aβ pathology was observed even in the presence of tau pathology.[179]

Certain chemical determinants have also been shown to be crucial to achieve LCOs that can be utilized for optical assignment of protein aggregates. In a study by Klingstedt and co-workers,[117] a library of anionic LCOs was synthesized and evaluated regarding their optical performances as amyloid ligands. For spectral differentiation of aggregated Aβ and tau species in AD brain tissue sections, an LCO having a backbone of at least five to seven thiophene units with carboxylic groups extending the conjugated backbone was needed. Moreover, detection of pre-fibrillar non-thioflavinophilic protein assemblies during *in vitro* fibril formation of recombinant Aβ 1–42

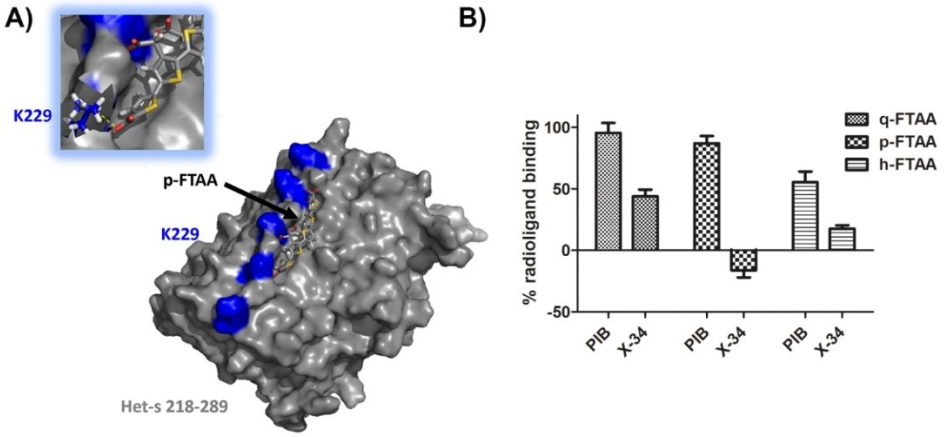

C)

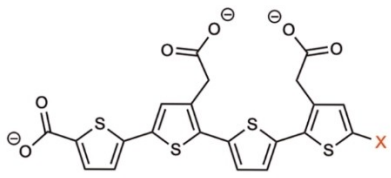

X	EC_{50} Values (nM) Synthetic Aβ1-42 fibrils	EC_{50} Values (nM) ADPBC
H	330–630	300–500
Br	20	2.2
I	90	50
NO_2	120	18
$CONH_2$	220	55
OMe	64	40
CO_2H	830	100
CN	15	<0.1

Figure 12. Binding modes of LCOs to protein aggregates. A) HADDOCK model (PDB ID: 2MUS) of p-FTAA (LIN5001) docked to HET-s(218-289)E265 K based on NMR-derived distance restraints. One of the key residues, K229, interacting with carboxylic acid side-chain groups of the ligand, is marked in blue. B) Displacement of ^{3}H-PIB or ^{3}H-X-34 from recombinant Aβ1–42 fibrils by three different LCOs, q-FTAA, p-FTAA and h-FTAA. C) Left: Chemical structure of q-FTAA analogues with different chemical moieties (X) in one of the α-terminal positions of the conjugated thiophene backbone. Right: EC_{50} values of q-FTAA analogues competing with ^{3}H-X-34 binding to synthetic recombinant Aβ 1–42 fibrils and AD brain-derived Aβ (ADPBC). Panel B reproduced from ref. [179] with permission. Panel C adapted from ref. [179] with permission.

could only be afforded by pentameric, hexameric and heptameric LCOs (Figure 13A).[117] Later, it was also revealed that the flexibility of the conjugated thiophene backbone was another important factor for achieving LCOs able to detect non-thioflavinophilic Aβ aggregates or non-congophilic prion aggregates, as well as spectrally discriminating Aβ and tau aggregates in tissue sections.[118] By replacing the central thiophene unit of p-FTAA with selenophene or phenylene, the conformational flexibility of the conjugated backbone was restricted. Ligands with these chemical modifications, p-FTAA-Se and p-FTAA-Ph, showed less spectral variation between Aβ and tau deposits in human AD tissue sections compared to p-FTAA. Furthermore, p-FTAA-Ph and p-FTAA-MeOPh (Figure 13B) failed to detect p-FTAA positive pre-fibrillar non-thioflavinophilic protein assemblies during *in vitro* fibril formation of recombinant Aβ 1–42, as well as p-FTAA positive non-congophilic prion aggregates (Figure 13C and D). In this study, the asymmetric tetrameric thiophene, HS-68, was also identified as a superior ligand for distinct spectral differentiation between aggregated Aβ and tau pathologies.[118] Thus, tetrameric LCOs with carboxylic groups extending the conjugated backbone could also be used for spectral differentiation of aggregated Aβ and tau species in human AD brain tissue sections. In addition, to the chemical determinants described above, distinct solvatochromic and viscosity-dependent behaviours of the ligands have also been shown to be important when designing improved LCOs for spectral separation of Aβ and tau deposits.[120]

As described earlier, HS-68 showed spectral variation assigned to age-dependent polymorphism of Aβ and tau aggregates in transgenic mouse models.[121] In this study, four analogues to HS-68 (Figure 14A), with small alterations in the chemical design, were also synthesized and examined regarding their possibility to spectrally discriminate between different

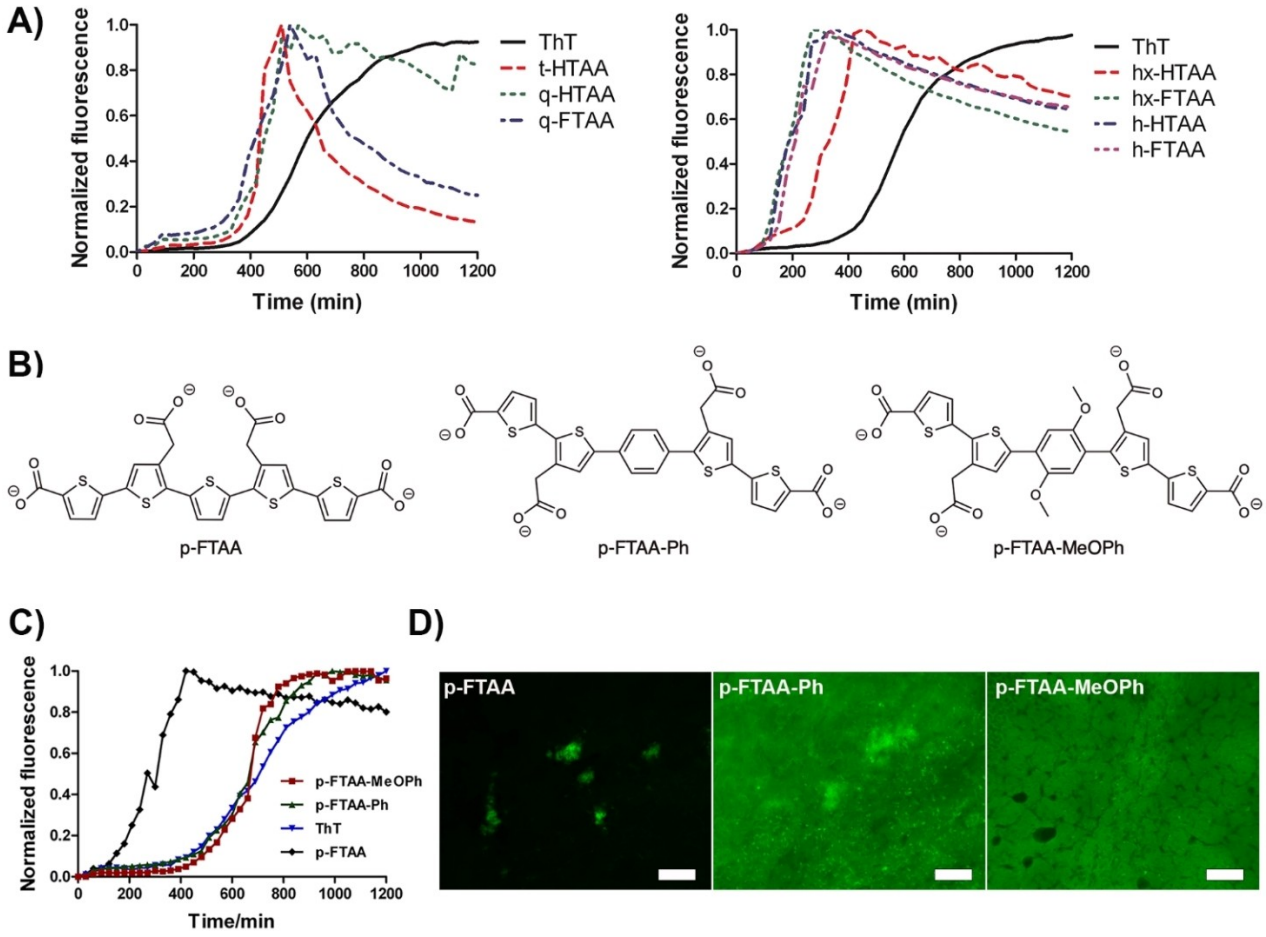

Figure 13. A certain length and conformational flexibility of the conjugated backbone are essential chemical determinants for achieving superior LCOs for optical assignment of protein aggregates. A) Fibril formation of recombinant Aβ1–42 monitored by fluorescence from ThT or LCOs. Left: Time plot showing the fibril formation kinetics of Aβ1–42 monitored by fluorescence from ThT, and the tetrameric LCOs, t-HTAA, q-HTAA or q-FTAA. Right: Time plot of Aβ1–42 fibril formation kinetics monitored by fluorescence from ThT, hx-HTAA, hx-FTAA, h-HTAA or h-FTAA. Both hexamers and heptamers detected non-thioflavinophilic species in the fibril formation pathway and showed initiation of the growth phase around 90 min, whereas tetramers (left) showed a similar onset as ThT. B) Chemical structures of p-FTAA, p-FTAA-Ph and p-FTAA-MeOPh. C) The fibril formation of recombinant Aβ1–42 monitored by fluorescence from ThT, p-FTAA, p-FTAA-Ph or p-FTAA-MeOPh. p-FTAA detects early non-thioflavinophilic species in the fibril formation pathway, whereas p-FTAA-Ph and p-FTAA-MeOPh showed an increase in emission at the same time as the onset of ThT. D) Images of brain sections from prion-infected transgenic mice stained with p-FTAA, p-FTAA-Ph or p-FTAA-MeOPh. Scale bars: 50 μm. Panel A reprinted from ref. [117] with permission from the Royal Society of Chemistry. Panels C, D reproduced from ref. [118] with permission.

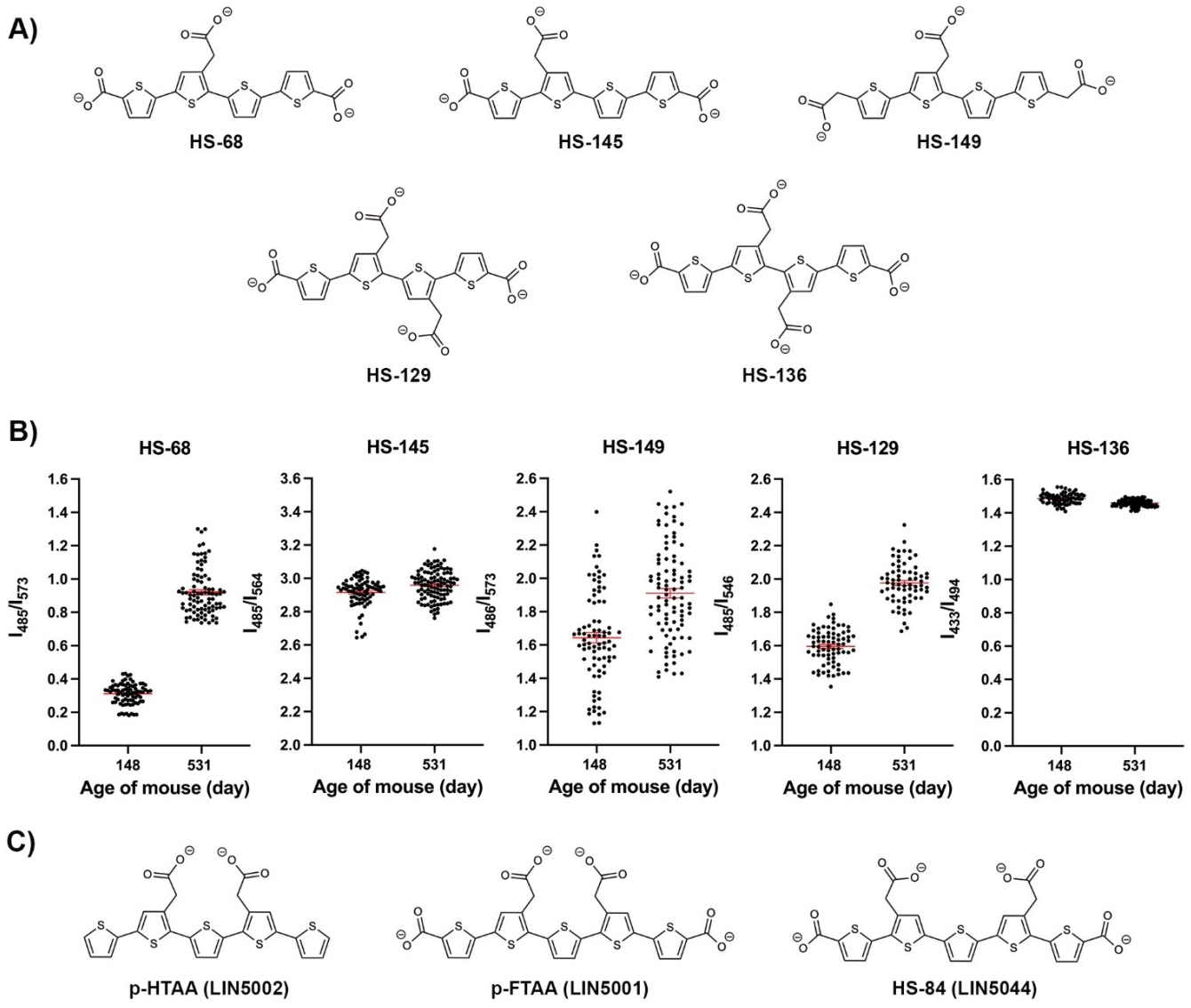

D)

LCO	α-terminal carboxylic groups	Periodicity of the anionic side chains	Prolonged survival (%)
p-HTAA (LIN5002)	no	5 Å	0
p-FTAA (LIN5001)	Yes	10 Å - 5 Å - 10 Å	36
HS-84 (LIN5044)	Yes	5 Å - 10 Å - 5 Å	> 80

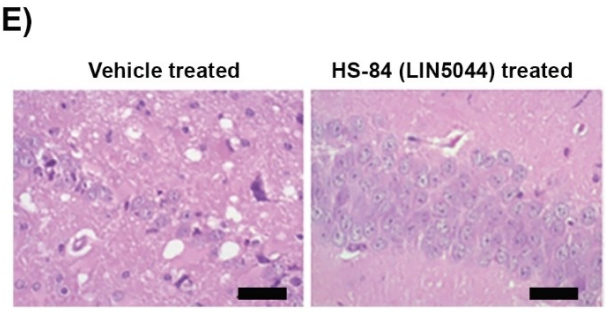

Figure 14. Distinct spacing of anionic groups along the conjugated backbone is an essential chemical determinant for achieving superior LCOs. A) Chemical structures of tetrameric LCOs with distinct spacing of anionic groups along the conjugated thiophene backbone. B) Spectral analyses of the tetrameric analogues bound to Aβ deposits in frozen brain sections from APPPS1 mice sacrificed at the indicated ages. The ratio plots were calculated from the emission intensity at the specified wavelengths for each LCO upon binding to Aβ deposits. The mean and standard error of the mean are indicated. C) Chemical structures of pentameric LCOs with distinct spacing of anionic groups along the conjugated thiophene backbone. D) Correlation between the chemical structure of pentameric LCOs and the therapeutic effect of the ligand, specified as prolonged survival, in prion infected mice. E) Histopathological analysis of brain sections from prion infected mice prophylactically treated with vehicle or HS-84 (LIN5044) and sacrificed at 63 days post infection. Neuronal cell loss and spongiform changes in CA1 of the hippocampus were consistently detected in vehicle-treated mice but were strongly reduced or absent in LIN5044-treated mice. Scale bars: 20 μm. Panel B adapted from ref. [121] with permission. Panel E reproduced from ref. [122] with permission.

aggregated morphotypes of Aβ and tau. By moving the acetate functional group on the second thiophene ring from position three to four, rendering ligand HS-145 (Figure 14 A), the ability to show age-dependent spectral difference of Aβ and tau aggregates was highly reduced (Figure 14B). In addition, exchanging the end carboxyl groups on HS-68 with acetate moieties, giving HS-149 (Figure 14A), or adding an acetate substituent on thiophene ring number three (HS-136 and HS-129; Figure 14A), also impaired the spectral separation of the aggregated morphotypes (Figure 14B). Hence, distinct spacing of anionic groups is an essential chemical determinant for achieving thiophene-based ligands that can distinguish polymorphic Aβ or tau aggregates. These findings are in line with the suggested binding mode of LCOs to protein aggregates,[122,175,176] as distinct interactions with the regularly spaced lysine residues along the fibrils will influence the conformation of the conjugated backbone and thereby the intrinsic photophysical properties of the ligand. The length of the conjugated backbone, as well as distinct spacing of anionic groups along the backbone, were also essential determinants for having LCOs exhibiting a therapeutic effect in prion infected mice.[122] In the study by Herrmann and co-workers, it was shown that an anti-prion activity required a minimum of five thiophene rings with regularly spaced carboxyl side groups. By administering the ligands to the brain using osmotic mini-pumps, the lead compound LIN5004, also known as HS-84 (Figure 14C), extended survival by $>80\%$ and showed activity against both mouse and hamster prions. A therapeutic effect was also observed upon intraperitoneal administration into mice. In contrast, the structurally related analogue p-FTAA (LIN5001) had a reduced effect, suggesting that the periodicity of the anionic side groups, ≈5 Å–10 Å–5 Å (HS-84) or ≈10 Å–5 Å–10 Å (p-FTAA), was important to result in an efficient anti-prion compound. In addition, for p-HTAA (LIN5002), a pentamer lacking the α-terminal carboxylic groups extending the conjugated backbone, the anti-prion effect was completely absent.[122] Thus, similar chemical determinants that have been shown to be important for accomplishing superior spectral assignment of protein aggregates seem to be essential for achieving a therapeutic effect of LCOs in prion infected mice. Distinct spacing of anionic groups along the backbone was also crucial for achieving heptameric D–A–D-based LCOs that could be used for spectral assignment of CAA or Aβ cored plaques in brain tissue sections from transgenic mouse models with Aβ pathology.[125]

Further correlations between ligand binding mode to distinct protein aggregates and chemical composition of the ligand were afforded when using proteophenes for staining of human AD brain tissue sections.[127] As mentioned above, proteophenes are the latest generation of LCOs with specific amino acid side-chain functionalization along the thiophene backbone. In addition to the α-carbon side chain from the amino acids, the carboxyl groups of the amino acids are also accessible since the amino acid was linked to the thiophene moieties with HATU-mediated amide coupling reactions.[127] Thus, similar to the anionic LCOs,[122,175,176] interactions between side-chain carboxyl groups with regularly spaced lysine residues in well-accessible grooves along the protein fibrils can be afforded. However, depending on the chemical nature of the α-carbon amino acid side chain, the interaction between the proteophene and the protein aggregate might be altered. In fact, when comparing staining with distinct proteophenes towards CAA, Aβ cored plaques, diffuse Aβ plaques and aggregated tau pathology, a variation in ligand binding towards these pathological entities could be observed.[127] HS-84-V-V, a proteophene with nonpolar isopropyl side chain from valine in both α-positions and β-positions along the thiophene backbone detected less aggregated species than ligands with charged, HS-84-E-E and HS-84-K-K, or uncharged polar, HS-84-Y-Y, side chains, from the amino acids in both the α-positions and β-positions (Figure 15). Moreover, proteophenes with uncharged or non-polar side chains in the α-positions and anionic polar side chains in the β-positions, HS-84-V-E and HS-84-Y-E, revealed intense staining of aggregated tau species, whereas a smaller amount or no observable staining of aggregated tau pathology was observed for proteophenes with anionic polar side chains in the α-positions and anionic, uncharged- or non-polar side chains in the β-positions, HS-84-E-E, HS-84-E-Y and HS-84-E-V (Figure 15). Thus, the chemical nature of the amino acid functionalities at the α- or β-positions along the thiophene backbone had a major impact on the proteophenes' ability to identify certain aggregated species in human AD brain tissue sections.[127]

Overall, the predicted binding mode, as well as the chemical determinants for superior optical ligands, have rendered mechanistic molecular insights regarding the performance of thiophene-based ligands for optical assignment of protein aggregates. Firstly, the selectivity of anionic LCPs and LCOs towards protein aggregates is presumably associated with the distinct binding site comprised of regularly spaced cationic residues situated in well-accessible grooves along the protein fibrils (Figure 12A). These grooves with repetitive cationic residues are most likely a common structural element for protein aggregates in general and are not abundant in native proteins. As the molecular interplay between the ligand and the protein fibril is dependent on electrostatic interactions between the anionic carboxylic groups of the ligand and the cationic lysine residues on the fibril, as well as on hydrophobic interactions between the thiophene backbone and the groove, ligands having a distinct molecular composition that is complementary to the binding site will have a higher selectivity and affinity. Thus, the LCOs, and the second generation of LCPs, most likely display a better selectivity towards protein aggregates compared to the first generation of polydispersed LCPs, as these ligands have a chemically defined composition matching the plausible binding site on the protein aggregate.

Secondly, the electrostatic interactions between the anionic carboxylic groups of the ligand and the cationic lysine residues on the fibril will govern the conformation of the conjugated thiophene backbone. By changing the torsion angle between adjacent thiophene units, the planarity of the conjugated thiophene backbone, as well as the photophysical properties of the ligand, are altered. In addition, a planarization of the backbone might also generate interchain energy transfer

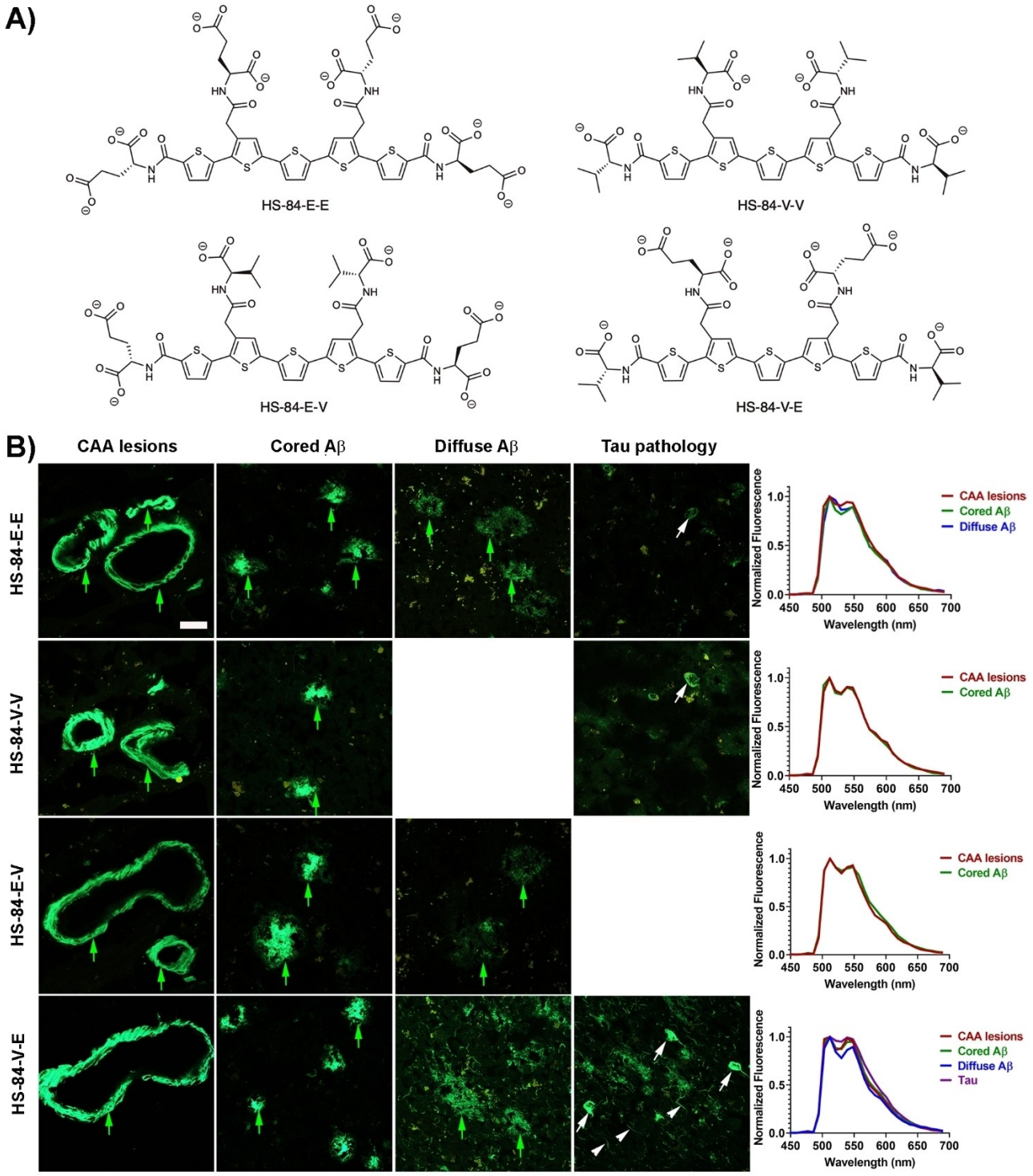

Figure 15. Proteophenes with distinct amino acid side-chain functionalities display different binding to aggregated Aβ and tau pathologies in human AD brain tissue sections. A) Chemical structure of the pentameric proteophenes, HS-84-E-E, HS-84-V-V, HS-84-E-V and HS-84-V-E. B) Fluorescence assignment of different Aβ and tau pathologies in human AD brain tissue sections stained with different proteophenes. Images and fluorescence spectra of immuno-positive Aβ deposits (green arrows), including cerebral amyloid angiopathy (CAA) lesions, Aβ cored plaques, diffuse Aβ plaques, and tau pathology (white arrows: neurofibrillary tangles (NFTs), white arrowheads: neuropil threads) in tissue sections stained with 100 nM HS-84-E-E, HS-84-V-V, HS-84-E-V or HS-84-V-E. Autofluorescence from lipofuscin is shown in yellow. Staining was performed on adjacent sections, and the images were recorded in spectral mode after excitation at 488 nm; the emission was collected between 450 and 700 nm. Scale bar: 20 μm. Adapted from ref. [127] with permission.

between adjacent bound ligands.[180] Hence, if the pattern of regularly spaced cationic residues differs between protein aggregates, distinct spectral signatures or fluorescent decays can be afforded from the bound ligand. Likewise, as observed

for HS-68 and the related analogues,[121] different spectral signatures could only be afforded for ligands having a distinct spacing of anionic group along the conjugated thiophene backbone. From a biomolecular perspective, an alteration of the LCO binding mode, and thereby the optical properties of the ligand, could be observed due to structural rearrangement of the protein aggregates, but it could also be associated with post-translational modification of the protein or the presence of other additional molecules in the protein aggregate. As mentioned above, protein aggregates associated with NDs display a structural diversity and these proteins are also susceptible to a wide range of post-translational modifications and different truncated versions of peptides/proteins are formed.[59–63] In some of the studies described above,[164–167] the observed spectral variations of the ligands were correlated with an alteration of the biochemical composition or the structure of the protein aggregates. However, to achieve even further molecular insight regarding the structural arrangement of protein aggregates that display distinct LCO spectral signatures, studies combining cryo-EM and hyperspectral microscopy are necessary. Clearly, the LCOs ligands can be used as optical tools to reveal an aggregate polymorphism when comparing protein aggregates within different samples, but additional tools and techniques are required to pin-point the molecular details underlying the polymorphism.

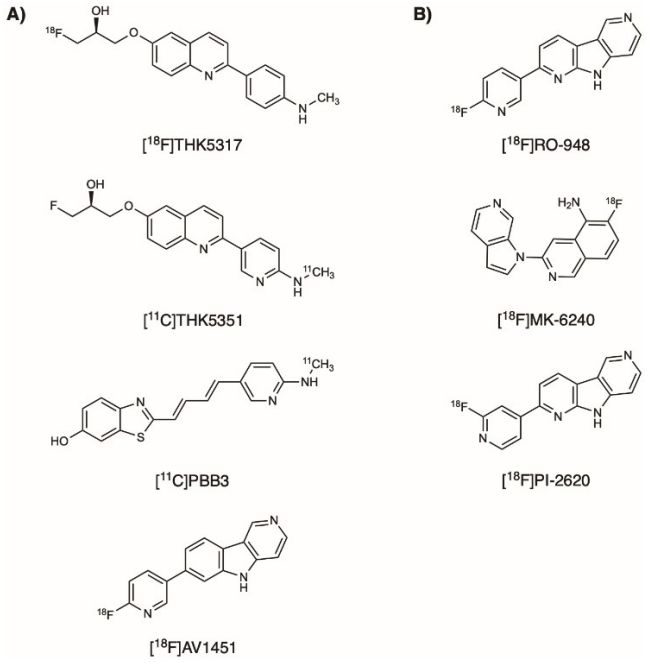

Figure 16. Different generations of PET tracers selectively targeting tau pathology. Chemical structures of the A) first and B) second generations of tau PET tracers.

6. The Next Generation of Thiophene-Based Ligands

Most of the ligands described so far detect disease-associated protein aggregates in general, but small molecular ligands that target specific disease-associated protein aggregates consisting of a distinct protein have also been presented. As mentioned above, various thioflavin analogues (Figure 2B) enabling visualization of Aβ deposits in humans with AD by PET imaging have been afforded.[80,84–88] Moreover, different generations of ligands selectively targeting tau pathology in AD have also been introduced (Figure 16).[181–189] However, several of these ligands display unspecific binding to other molecular targets, as well as limited selectivity towards the distinct tau aggregates found in specific tauopathies.[190–194] Thus, tau PET imaging in neurodegenerative tauopathies is still a challenge and development of novel ligands is essential for accurate diagnostic of individual tauopathies. Efforts towards the development of PET tracers for α-syn aggregates have proven to be even more challenging, mainly due to low abundance of α-syn aggregates within the brain, as well as difficulties in achieving ligand selectivity towards α-syn pathology.[195] Today, efficient PET tracers for clinical imaging of α-syn aggregates are lacking.

Recently, a novel generation of thiophene-based ligands selectively targeting Aβ or tau pathology in human AD brain tissue sections was presented.[196,197] Ligands targeting tau pathology were afforded by mimicking the previously reported first-generation tau ligand, PBB3 (Figure 16A).[185] By replacing the pyridinyl-butadienyl-motif of PBB3 with bi-thiophene-vinyl moieties, a set of compounds denoted bi-thiophene-vinyl-benzothiazoles/benzothiazoliums (bTVBTs) was afforded, and this class of ligands showed bright fluorescence from aggregated tau species in AD brain tissue sections, whereas staining of Aβ pathology was absent.[196] In contrast, for a second class of compounds, denoted *tert*-thiophene-benzothiazoles (tTBTs), having the pyridinyl-butadienyl-motif of PBB3 replaced with different *tert*-thiophene motifs, staining of both immunopositive Aβ aggregates and aggregated tau pathology was lacking. Moreover, compound bTVBI1, which had a benzimidazole moiety, 1-ethyl-1*H*-benzimidazole, instead of a benzothiazole/benzothiazolium attached to the bi-thiophene-vinyl moiety, displayed staining towards immuno-positive Aβ aggregates, as well as some weak staining of tau-like pathology. Thus, minor chemical alterations of the bTVBT scaffold abolished the selectivity towards tau pathology.[196] The binding mode of b-TVBT ligands to tau aggregates has also been studied by a combination of theoretical methods and experimental spectroscopies.[198] With reference to the AD tau structure obtained by cryo-EM,[45] a periodic model system of the tau fibril was generated, and the interactions between this fibril and the ligand bTVBT4 were studied with nonbiased molecular dynamics simulations. These studies revealed that the most favourable ligand-protein binding occurred at the hydrophobic pocket defined by residues Ile360, Thr361, and His362 (Figure 17B).[198] In addition, the theoretical absorption spectrum of bTVBT4 bound to this region was similar to the experimental absorption spectrum obtained from the ligand bound to NFTs in tissue sections. When comparing the cryo-EM structure of tau fibrils purified from the brain of a patient with PiD with the structure

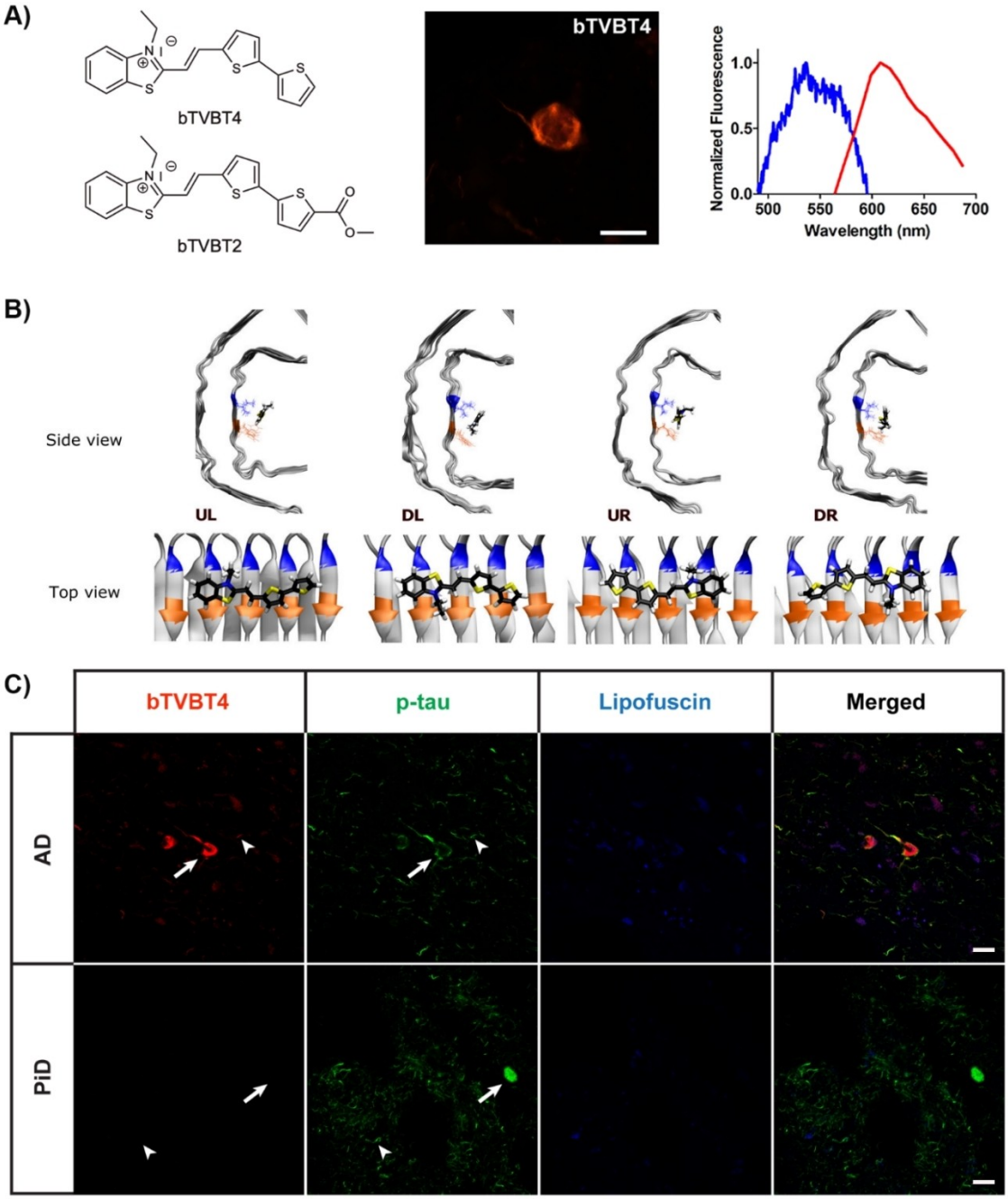

Figure 17. Next generation of thiophene-based ligands that selectively stain aggregated tau pathology in human AD brain tissue sections. A) Chemical structures of tau-selective ligands bTVBT4 and bTVBT2 (left). Image of a neurofibrillary tangle (NFT) stained by bTVBT4 (middle); scale bar: 10 μm, and excitation (blue) and emission (red) spectra of bTVBT4 when bound to tau aggregates in human AD brain tissue sections (right). B) Identified binding modes for bTVBT4 to AD tau aggregates during molecular dynamic simulations, with separation of down (D), up (U), left (L), and right (R) orientation of the ethyl group with respect to His362 (orange) and Ile360 (blue). C) Fluorescence images of brain tissue sections from a patient diagnosed with Alzheimer's disease (AD, top) or Pick's disease (PiD, bottom) stained with 100 nM bTVBT4 (red) and phospho-tau antibody AT8 (p-tau, green). Arrow: neurofibrillary tangle (AD), Pick body (PiD). Arrowhead: neuropil thread. As the autofluorescence from lipofuscin granules can overlap with bTVBT4 emission, an additional channel in which the settings only allowed excitation of lipofuscin (blue) is also shown. Scale bars: 20 μm. Panel A reproduced from ref. [196] with permission. Panels B, C adapted from ref. [198] with permission under Creative Commons Attribution 4.0 International License (http://creativecommons.org/licenses/by/4.0/). Copyright: 2021, The Authors.

of AD tau (Figure 1),[45,46] the proposed bTVBT4 binding site was not present in the PiD fold. Furthermore, fluorescence imaging of bTVBT4 stained brain tissue samples from patients diagnosed with AD or PiD revealed clear staining of aggregated tau pathologies in AD, whereas bTVBT4 staining of immuno-positive tau aggregates in PiD was lacking (Figure 17C).[198] Thus, the bTVBTs seem to be rather selective for AD tau pathology and, in

addition, the observations provide strong support for the suggested AD tau binding site of the ligands.

Thiophene-based ligands using the second-generation tau ligand, MK-6240 (Figure 16B),[188,189] as a template have also been reported.[197] Surprisingly, when replacing the 5-amino-isoquinoline motif of MK-6240 with a methyl-bithiophene-carboxylate building block, the resulting ligand, HS-276 (Figure 18A), showed high selectivity for aggregated Aβ pathologies. When staining human AD brain tissue section with HS-276, bright fluorescence from cored Aβ plaques and diffuse plaques in the grey matter, as well as Aβ deposits in the white matter, could be observed, whereas staining of the classical tau pathologies, such as NFTs and dystrophic neurites was lacking (Figure 18B).[197] In the bTVBT family, the tau selective ligand bTVBT2 (Figure 17A) has the same bithiophene building block as HS-276, but it is attached to a benzothiazolium moiety instead of an azaindole unit. Thus, by combining the bithiophene building block with different chemical moieties, selectiv-

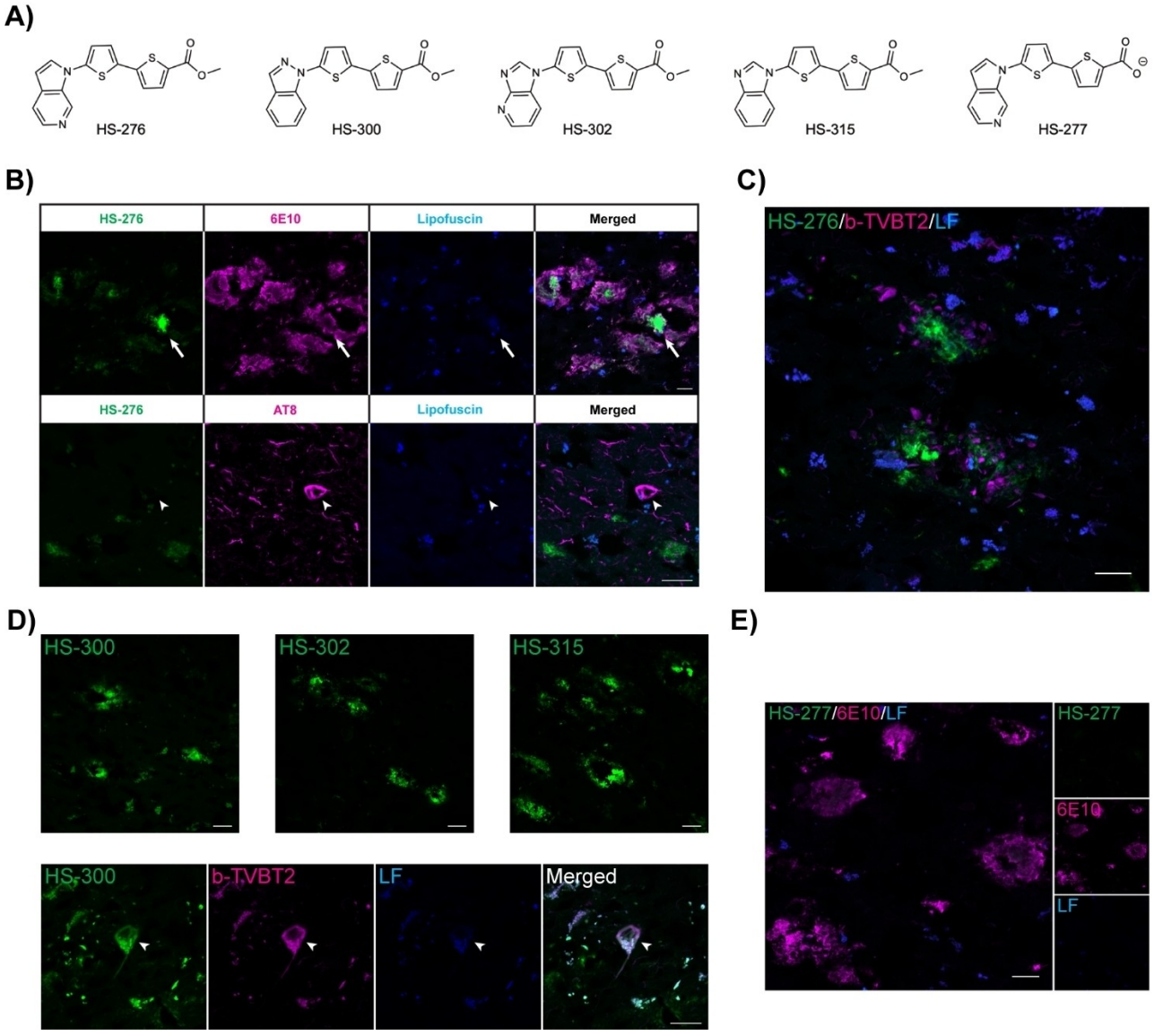

Figure 18. The next generation of thiophene-based ligands that selectively stain aggregated Aβ pathology in human AD brain tissue sections. A) Chemical structures of ligands HS-276, HS-300, HS-302, HS-315 and HS-277. B) Fluorescence images of AD brain tissue sections labelled with anti-Aβ-antibody (magenta, 6E10) and HS-276 (green; top) or ant-phospho-tau (p-tau) antibody (magenta, AT8) and HS-276 (green; bottom). HS-276 showed co-localization with the 6E10 antibody (white arrows), whereas HS-276 staining of immuno-positive tau aggregates, such as NFTs (white arrow heads), was lacking. Autofluorescent lipofuscin is shown in blue; scale bars: 20 μm. C) Fluorescence image of AD brain section stained with HS-276 and bTVBT2 simultaneously. The emission from H-276 (green) and bTVBT2 (magenta) could be separated into two channels; this allowed differentiation of Aβ and tau pathology based on the colour of the emitted light. Autofluorescence from lipofuscin granules (LF) is also displayed (blue); scale bar, 20 μm. D) Fluorescence images of Aβ aggregates (green) stained by HS-300, HS-302 or HS-315 (top). Fluorescence image of AD brain tissue section doubly labelled with HS-300 (green) and bTVBT2 (magenta). HS-300 co-localized with bTVBT2, confirming that the ligand was binding to tau inclusions. Autofluorescence from LF is depicted in blue; scale bars: 20 μm. E) Fluorescence images of AD brain tissue section doubly stained with anti-Aβ-antibody (magenta, 6E10) and HS-277 (green). In contrast to the methylated analogue (HS-276), HS-277 did not stain Aβ deposits. Autofluorescence from lipofuscin is shown in blue; scale bar: 20 μm. Panels B-E adapted from ref. [197] with permission.

ity towards aggregated tau or Aβ pathologies could be achieved, and bTVBT2 and HS-276 could be used for optical assignment of the aggregated species in human AD brain tissue sections (Figure 18C). Ligands having the azaindole unit replaced by similar nitrogen containing heterocyclic aromatic compounds (Figure 18A), such as indazole (HS-300), azabenzimidazole (HS-302), or benzimidazole (HS-315), also displayed staining towards aggregated Aβ pathologies. However, for these ligands, labelling of NFTs and dystrophic neurites could also be observed to some extent (Figure 18D).[197] Hence, the positional changes of the heterocyclic nitrogen atoms did not impact Aβ binding but influenced ligand labelling of tau aggregates. Moreover, demethylation of the methyl-bithiophene-carboxylate building block resulted in loss of binding to Aβ deposits, except when the bi-thiophene moiety was attached to an indazole unit. As shown for HS-277, the demethylated analogue to HS-276, staining of immuno-positive Aβ deposits was lacking (Figure 18E). Thus, the presence of anionic groups on the thiophene building blocks was unfavourable for the interaction with protein aggregates, which is in contrast to the observations with the LCOs. Overall, the chemical combination of LCO thiophene building blocks with other heterocyclic moieties has generated a novel generation of protein aggregate selective ligands that can be used for optical assignment of protein aggregates in tissue sections.[196–198] Furthermore, subtle chemical alterations of the ligands have a major impact on the protein aggregate selectivity and these ligand scaffolds can be further explored for the development of tracers for clinical PET imaging.

7. Summary and Outlook

Ligands that can detect polymorphic protein aggregates are essential to give insight into the basic mechanisms of the pathogenesis of distinct diseases, as well as to aid in accurate diagnosis of these disorders. Clearly, the thiophene-based ligands described above have been implemented as fluorescent tools for assessing these shape-shifting aggregated pathological species within different model systems and patient-derived materials. Furthermore, these ligands have been used to show aggregate polymorphism that can be assigned to different biological and pathological phenomena, such as age-related changes of the protein aggregates or specific aggregate species in distinct diseases. These phenomena have been revealed by hyperspectral and fluorescent lifetime imaging, as the intrinsic conformation-sensitive photophysical properties of thiophene-based ligands generate distinct optical fingerprints depending on the binding mode of the ligand. From a chemical perspective, minor chemical alterations of the ligands have been shown to influence both the binding mode and the optical performance of the ligands.

In this regard, further evolution of the ligands with an enhanced chemical diversity is of great interest as such ligands will most likely aid in revealing even more types of aggregate polymorphism, as well as generate novel molecular insight regarding the basic mechanisms of the shape-shifting properties of misfolded proteins, their spreading pathways and role in the pathogenesis of specific diseases. In addition, designing ligands with distinct emissions profiles in the near-infrared (NIR) range that can be used for NIR fluorescence imaging would also be of great interest.[100] Such ligands could for instance be afforded by generating similar D–A–D thiophene-based ligands, such as HS-169, LL-3 or LL-5 (Figure 4) with other acceptor molecules than BTD.

The chemical design of novel ligands will also be vital for accurate clinical diagnostics of a specific protein aggregation disease, and from this perspective, it will be interesting to convert the recently presented generation of thiophene-based ligands selective for distinct aggregated pathologies, such as Aβ or tau deposits, into radiolabelled tracers that can be used for PET imaging. Moreover, developing novel chemical scaffolds selectively targeting tau aggregates in other tauopathies than AD, as well as α-syn aggregates in MSA and PD, or the protein deposits associated with a specific type of systemic amyloidosis would also be of great interest. In this regard, high-resolution structures for a diversity of protein aggregates, recently provided by cryo-EM, will most likely assist in the chemical design of ligands with a distinct binding mode to a specific protein aggregate. As shown for the bTVBT ligands described above, such selective binding modes can be assessed by combining a diversity of theoretical and experimental methodologies.

An additional future research direction for the chemical design of thiophene-based ligands that can aid in combating protein-aggregation diseases is to continue to explore the therapeutic effect of these compounds. Clearly, the development of disease-modifying therapies that target Aβ or tau aggregates in AD is extremely challenging. So far, both immunotherapy and small-molecule-based enzyme and aggregation modulators have shown limited success in clinical trials. As shown above, properly functionalized LCOs exhibit an anti-prion activity, whereas closely related chemical analogues displayed no activity.[122] Furthermore, thiophene-based molecules have also been shown to act as dual modulators of Aβ and tau aggregation.[199] Hence, the development of small libraries of chemically defined thiophene-based ligands, targeting a variety of proteinaceous pathological species will be vital to unravelling the type of precision pharmacology that is needed for new therapies targeting protein aggregates. Overall, we foresee that further chemical development of thiophene-based ligands will continue to facilitate the molecular understanding of protein-aggregation diseases, as well as aid in combating these disorders.

Acknowledgements

Our work is supported by the Swedish Research Council (2016-00748), the Swedish Brain Foundation, Konung Gustaf V:s och Drottning Victorias Frimurarestiftelse and the U.S. National Institutes of Health (U01NS110437). The graphics in Table of Content was created with BioRender.com.

Conflict of Interests

The authors declare no conflict of interest.

Data Availability Statement

Data sharing is not applicable to this article as no new data were created or analyzed in this study.

Keywords: amyloid · fluorescent ligands · oligothiophenes · polymorphism · protein aggregation

[1] M. D. Benson, J. N. Buxbaum, D. S. Eisenberg, G. Merlini, M. J. M. Saraiva, Y. Sekijima, J. D. Sipe, P. Westermark, *Amyloid.* **2020**, *27*, 217–222.
[2] M. Sunde, C. Blake, *Adv. Protein Chem.* **1997**, *50*, 123–159.
[3] A. T. Petkova, Y. Ishii, J. J. Balbach, O. N. Antzutkin, R. D. Leapman, F. Delaglio, R. Tycko, *Proc. Natl. Acad. Sci. USA* **2002**, *99*, 16742–16747.
[4] C. Ritter, M. L. Maddelein, A. B. Siemer, T. Lührs, M. Ernst, B. H. Meier, S. J. Saupe, R. Riek, *Nature* **2005**, *435*, 844–848.
[5] O. S. Makin, E. Atkins, P. Sikorski, J. Johansson, L. C. Serpell, *Proc. Natl. Acad. Sci. USA* **2005**, *102*, 315–320.
[6] R. Nelson, M. R. Sawaya, M. Balbirnie, A. Ø. Madsen, C. Riekel, R. Grothe, D. Eisenberg, *Nature* **2005**, *435*, 773–778.
[7] H. Braak, E. Braak, *Neurobiol. Aging* **1997**, *18*, 351–357.
[8] J. L. Price, J. C. Morris, *Ann. Neurol.* **1999**, *45*, 358–368.
[9] C. R. Jack, V. J. Lowe, S. D. Weigand, H. J. Wiste, M. L. Senjem, D. S. Knopman, M. M. Shiung, J. L. Gunter, B. F. Boeve, B. J. Kemp, M. Weiner, R. C. Petersen, Alzheimer's Disease Neuroimaging Initiative, *Brain* **2009**, *132*, 1355–1365.
[10] C. R. Jack, D. S. Knopman, W. J. Jagust, L. M. Shaw, P. S. Aisen, M. W. Weiner, R. C. Petersen, J. Q. Trojanowski, *Lancet Neurol.* **2010**, *9*, 119–128.
[11] R. Bateman, C. Xiong, T. L. S. Benzinger, A. M. Fagan, A. Goate, N. C. Fox, D. S. Marcus, N. G. Cairns, X. Xie, T. M. Blazey, D. M. Holtzman, A. Santacruz, V. Buckles, A. Oliver, K. Moulder, P. S. Aisen, B. Ghetti, W. E. Klunk, E. McDade, R. N. Martins, C. L. Masters, R. Mayeux, J. M. Ringman, M. N. Rossor, P. R. Schofield, R.A Sperling, S. Salloway, J. C. Morris, Dominantly Inherited Alzheimer Network, *N. Engl. J. Med.* **2012**, *367*, 795–804.
[12] S. Furumoto, N. Okamura, R. Iwata, K. Yanai, H. Arai, Y. Kudo, *Curr. Top. Med. Chem.* **2007**, *7*, 1773–1789.
[13] K. P. R. Nilsson, *FEBS Lett.* **2009**, *583*, 2593–2599.
[14] A. A. Reinke, J. E. Gestwicki, *Chem. Biol. Drug Des.* **2011**, *77*, 399–411.
[15] J. S. Pedersen, C. B. Andersen, D. E. Otzen, *FEBS J.* **2010**, *27*, 4591–4601.
[16] M. Fändrich, S. Nyström, K. P. R. Nilsson, A. Böckmann, H. LeVine III, P. Hammarström, *J. Intern. Med.* **2018**, *283*, 218–237.
[17] R. Tycko, *Neuron* **2015**, *86*, 632–645.
[18] J. Adamcik, R. Mezzenga, *Angew. Chem. Int. Ed. Engl.* **2018**, *57*, 8370–8382.
[19] M. G. Iadanza, M. P. Jackson, E. W. Hewitt, N. A. Ranson, S. E. Radford, *Nat. Rev. Mol. Cell Biol.* **2018**, *19*, 755–773.
[20] M. Doran, D. G. du Plessis, T. P. Enevoldson, N. A. Fletcher, E. Ghadiali, A. J. Larner, *J. Neurol. Sci.* **2003**, *216*, 127–134.
[21] B. Lam, M. Masellis, M. Freedman, D. T. Stuss, S. E. Black, *Alzheimer's Res. Ther.* **2013**, *5*, 1.
[22] N. S. Ryan, J. M. Nicholas, P. S. J. Weston, Y. Liang, T. Lashley, R. Guerreiro, G. Adamson, J. Kenny, J. Beck, L. Chavez-Gutierrez, B. de Strooper, T. Revesz, J. Holton, S. Mead, M. N. Rossor, N. C. Fox, *Lancet Neurol.* **2016**, *15*, 1326–1335.
[23] N. M. E. Scheltens, F. Galindo-Garre, Y. A. L. Pijnenburg, A. E. van der Vlies, L. L. Smits, T. Koene, C. E. Teunissen, F. Barkhof, M. P. Wattjes, P. Scheltens, W. M. van der Flier, *J. Neurol. Neurosurg. Psychiatry* **2016**, *87*, 235–243.
[24] F. Clavaguera, H. Akatsu, G. Fraser, R. A. Crowther, S. Frank, J. Hench, A. Probst, D. T. Winkler, J. Reichwald, M. Staufenbiel, B. Ghetti, M. Goedert, M. Tolnay, *Proc. Natl. Acad. Sci. USA* **2013**, *110*, 9535–9540.
[25] D. Eisenberg, M. Jucker, *Cell* **2012**, *148*, 1188–1203.
[26] H. Levine 3rd, L. C. Walker, *Neurobiol. Aging* **2010**, *31*, 542–548.
[27] M. Jucker, L. C. Walker, *Nat. Neurosci.* **2018**, *21*, 1341–1349.
[28] B. H. Toyama, J. S. Weissman, *Annu. Rev. Biochem.* **2011**, *80*, 557–585.
[29] J. Collinge, A. R. Clarke, *Science* **2007**, *318*, 930–936.
[30] C. L. Maarouf, I. D. Daugs, S. Spina, R. Vidal, T. A. Kokjohn, R. L Patt, W. M. Kalback, D. C. Luehrs, D. G. Walker, E. M. Castaño, T. G Beach, B. Ghetti, A. E. Roher, *Mol. Neurodegener.* **2008**, *3*, 20.
[31] G. Heilbronner, Y. S. Eisele, F. Langer, S. A. Kaeser, R. Novotny, A. Nagarathinam, A. Åslund, P. Hammarström, K. P. R. Nilsson, M. Jucker, *EMBO Rep.* **2013**, *14*, 1017–1022.
[32] S. Nyström, K. M. Psonka-Antonczyk, P. G. Ellingsen, L. B. Johansson, N. Reitan, S. Handrick, S. Prokop, F. L. Heppner, B. M. Wegenast-Braun, M. Jucker, M. Lindgren, B. T. Stokke, P. Hammarström, K. P. R. Nilsson, *ACS Chem. Biol.* **2013**, *8*, 1128–1133.
[33] J. Rasmussen, J. Mahler, N. Beschorner, S. A. Kaeser, L. M. Häsler, F. Baumann, S. Nyström, E. Portelius, K. Blennow, T. Lashley, N. C. Fox, D. Sepulveda-Falla, M. Glatzel, A. L. Oblak, B. Ghetti, K. P. R. Nilsson, P. Hammarström, M. Staufenbiel, L. C. Walker, M. Jucker, *Proc. Natl. Acad. Sci. USA* **2017**, *114*, 13018–13023.
[34] C. Condello, T. Lemmin, J. Stöhr, M. Nick, Y. Wu, A. M. Maxwell, J. C. Watts, C. D. Caro, A. Oehler, C. D. Keene, T. D. Bird, S. G. van Duinen, L. Lannfelt, M. Ingelsson, C. Graff, K. Giles, W. F. DeGrado, S. B. Prusiner, *Proc. Natl. Acad. Sci. USA* **2018**,*115*, E782–E791.
[35] A. T. Petkova, R. D. Leapman, Z. Guo, W–M. Yau, M. P. Mattson, R. Tycko, *Science* **2005**, *307*, 262–265.
[36] M. Meyer-Luehmann, J. Coomaraswamy, T. Bolmont, S. Kaeser, C. Schaefer, E. Kilger, A. Neuenschwander, D. Abramowski, P. Frey, A. L. Jaton, J–M. Vigouret, P. Paganetti, D. M. Walsh, P. M. Mathews, J. Ghiso, M. Staufenbiel, L. C. Walker, M. Jucker, *Science* **2006**, *313*, 1781–1784.
[37] J–X. Lu, W. Qiang, W-M. Yau, C. D. Schwieters, S. C. Meredith, R. Tycko, *Cell* **2013**, *154*, 1257–1268.
[38] J. C. Watts, C. Condello, J. Stöhr, A. Oehler, J. Lee, S. J. DeArmond, L. Lannfelt, M. Ingelsson, K. Giles, S. B. Prusiner, *Proc. Natl. Acad. Sci. USA* **2014**, *111*, 10323–10328.
[39] W. Qiang, W-M. Yau, J-X. Lu, J. Collinge, R. Tycko, *Nature* **2017**, *541*, 217–221.
[40] U. Ghosh, W-M. Yau, J. Collinge, R. Tycko, *Proc. Natl. Acad. Sci. USA* **2021**, *118*, e2111863118.
[41] M. Kollmer, W. Close, L. Funk, J. Rasmussen, A. Bsoul, A. Schierhorn, M. Schmidt, C. J. Sigurdson, M. Jucker, M. Fändrich, *Nat. Commun.* **2019**, *10*, 4760.
[42] Y. Yang, D. Arseni, W. Zhang, M. Huang, S. Lövestam, M. Schweighauser, A. Kotecha, A. G. Murzin, S. Y. Peak-Chew, J. Macdonald, I. Lavenir, H. J. Garringer, E. Gelpi, K. L. Newell, G. G. Kovacs, R. Vidal, B. Ghetti, B. Ryskeldi-Falcon, S. H. W. Scheres, M. Goedert, *Science* **2022**, *375*, 167–172.
[43] G. G. Kovacs, B. Ghetti, M. Goedert, *Neuropathol. Appl. Neurobiol.* **2022**, *48*, e12792.
[44] R. A. Crowther, M. Goedert, *J. Struct. Biol.* **2000**, *130*, 271–279.
[45] A. W. P. Fitzpatrick, B. Falcon, S. He, A. G. Murzin, G. Murshudov, H. J. Garringer, R. A. Crowther, B. Ghetti, M. Goedert, S. H. W. Scheres, *Nature* **2017**, *547*, 185–190.
[46] B. Falcon, W. Zhang, A. G. Murzin, G. Murshudov, H. J. Garringer, R. Vidal, R. A. Crowther, B. Ghetti, S. H. W. Scheres, M. Goedert, *Nature* **2018**, *561*, 137–140.
[47] B. Falcon, J. Zivanov, W. Zhang, A. G. Murzin, H. J. Garringer, R. Vidal, R. A. Crowther, K. L. Newell, B. Ghetti, M. Goedert, S. H. W. Scheres, *Nature* **2019**, *568*, 420–423.
[48] W. Zhang, A. Tarutani, K. L. Newell, A. G. Murzin, T. Matsubara, B. Falcon, R. Vidal, H. J. Garringer, Y. Shi, T. Ikeuchi, S. Murayama, B. Ghetti, M. Hasegawa, M. Goedert, S. H. W. Scheres, *Nature* **2020**, *580*, 283–287.
[49] Y. Shi, W. Zhang, Y. Yang, A. G. Murzin, B. Falcon, A. Kotecha, M. van Beers, A. Tarutani, F. Kametani, H. J. Garringer, R. Vidal, G. I. Hallinan, T. Lashley, Y. Saito, S. Murayama, M. Yoshida, H. Tanaka, A. Kakita, T. Ikeuchi, A. C. Robinson, D. M. A. Mann, G. G. Kovacs, T. Revesz, B. Ghetti, M. Hasegawa, M. Goedert, S. H. W. Scheres, *Nature* **2021**, *598*, 359–363.
[50] W. Zhang, B. Falcon, A. G. Murzin, J. Fan, R. A. Crowther, M. Goedert, S. H. W. Scheres, *eLife* **2019**, *5*, e43584.
[51] M. G. Spillantini, M. L. Schmidt, V. M. Lee, J. Q. Trojanowski, R. Jakes, M. Goedert, *Nature* **1997**, *88*, 839–840.
[52] M. G. Spillantini, R. A. Crowther, R. Jakes, N. J. Cairns, P. L. Lantos, M. Goedert, *Neurosci. Lett.* **1998**, *251*, 205–208.

[53] P. H. Tu, J. E. Galvin, M. Baba, B. Giasson, T. Tomita, S. Leight, S. Nakajo, T. Iwatsubo, J. Q. Trojanowski, V. M. Lee, *Ann. Neurol.* **1998**, *44*, 415–422.
[54] K. Wakabayashi, M. Yoshimoto, S. Tsuji, H. Takahashi, *Neurosci. Lett.* **1998**, *249*, 180–182.
[55] M. G. Spillantini, R. A. Crowther, R. Jakes, M. Hasegawa, M. Goedert, *Proc. Natl. Acad. Sci. USA* **1998**, *95*, 6469–6473.
[56] R. A. Crowther, S. E. Daniel, M. Goedert, *Neurosci. Lett.* **2000**, *292*, 128–130.
[57] Y. Yang, Y. Shi, M. Schweighauser, X. Zhang, A. Kotecha, A. G. Murzin, H. J. Garringer, P. W. Cullinane, Y. Saito, T. Foroud, T. T. Warner, K. Hasegawa, R. Vidal, S. Murayama, T. Revesz, B. Ghetti, M. Hasegawa, T. Lashley, S. H. W. Scheres, M. Goedert, *Nature* **2022**, *610*, 791–795.
[58] M. Schweighauser, Y. Shi, A. Tarutani, F. Kametani, A. G. Murzin, B. Ghetti, T. Matsubara, T. Tomita, T. Ando, K. Hasegawa, S. Murayama, M. Yoshida, M. Hasegawa, S. H. W. Scheres, M. Goedert, *Nature* **2020**, *585*, 464–469.
[59] L. Buee, T. Bussiere, V. Buee-Scherrer, A. Delacourte, P. R. Hof, *Brain Res. Brain Res. Rev.* **2000**, *33*, 95–130.
[60] C. Alquezar, S. Arya, A. W. Kao, *Front. Neurobiol.* **2021**, *7*, 595532.
[61] F. Prelli, E. Castaño, G. G. Glenner, B. Frangione, *J. Neurochem.* **1988**, *51*, 648–651.
[62] D. M. A. Mann, T. Iwatsubo, Y. Ihara, N. J. Cairns, P. L. Lantos, N. Bogdanovic, L. Lannfelt, B. Winblad, M. L. C. Maat-Schieman, M. N. Rossor, *Am. J. Pathol.* **1996**, *148*, 1257–1266.
[63] E. Gkanatsiou, E. Portelius, C. E. Toomey, K. Blennow, H. Zetterberg, T. Lashley, G. Brinkmalm, *Neurosci. Lett.* **2019**, *701*, 125–131.
[64] F. Liberta, S. Loerch, M. Rennegarbe, A. Schierhorn, P. Westermark, G. T. Westermark, B. P. C. Hazenberg, N. Grigorieff, M. Fändrich, M. Schmidt, *Nat. Commun.* **2019**, *10*, 1104.
[65] P. Swuec, F. Lavatelli, M. Tasaki, C. Paissoni, P. Rognoni, M. Maritan, F. Brambilla, P. Milani, P. Mauri, C. Camilloni, G. Palladini, G. Merlini, S. Ricagno, M. Bolognesi, *Nat. Commun.* **2019**, *10*, 1269.
[66] L. Radamaker, Y. H. Lin, K. Annamalai, S. Huhn, U. Hegenbart, S. O. Schönland, G. Fritz, M. Schmidt, M. Fändrich, *Nat. Commun.* **2019**, *10*, 1103.
[67] M. Schmidt, S. Wiese, V. Adak, J. Engler, S. Agarwal, G. Fritz, P. Westermark, M. Zacharias, M. Fändrich, *Nat. Commun.* **2019**, *10*, 5008.
[68] U. Cendrowska, P. J. Silva, N. Ait-Bouziad, M. Müller, Z. P. Guven, S. Vieweg, A. Chiki, L. Radamaker, S. T. Kumar, M. Fändrich, F. Tavanti, M. C. Menziani, A. Alexander-Katz, F. Stellacci, H. A. Lashuel, *Proc. Natl. Acad. Sci. USA* **2020**,*117*, 6866–6874.
[69] L. Radamaker, S. Karimi-Farsijani, G. Andreotti, J. Baur, M. Neumann, S. Schreiner, N. Berghaus, R. Motika, C. Haupt, P. Walther, V. Schmidt, S. Huhn, U. Hegenbart, S. O. Schönland, S. Wiese, C. Read, M. Schmidt, M. Fändrich, *Nat. Commun.* **2021**, *12*, 6434.
[70] M. Steinebrei, J. Gottwald, J. Baur, C. Röcken, U. Hegenbart, S. Schönland, M. Schmidt, *Nat. Commun.* **2022**, *13*, 6398.
[71] H. Bennhold, *Muench. Med. Wochenschr.* **1922**, *44*, 1537–1538.
[72] A. K. Schütz, A. Soragni, S. Hornemann, A. Aguzzi, M. Ernst, A. Böckmann, B. H. Meier, *Angew. Chem. Int. Ed.* **2011**, *50*, 5956–5960; *Angew. Chem.* **2011**, *123*, 6078–6082.
[73] W. E. Klunk, M. L. Debnath, J. W. Pettegrew, *Neurobiol. Aging* **1994**, *15*, 691–698.
[74] S. D. Styren, R. L. Hamilton, G. C. Styren, W. E. Klunk, *J. Histochem. Cytochem.* **2000**, *48*, 1223–1232.
[75] W. E. Klunk, B. J. Bacskai, C. A. Mathis, S. T. Kajdasz, M. E. McLellan, M. P. Frosch, M. L. Debnath, D. P. Holt, Y. Wang, B. T. Hyman, *J. Neuropathol. Exp. Neurol.* **2002**, *61*, 797–805.
[76] M. D. Ikonomovic, E. E. Abrahamson, B. A. Isanski, M. L. Debnath, C. A. Mathis, S. T. Dekosky, W. E. Klunk, *Methods Enzymol.* **2006**, *412*, 123–144.
[77] R. P. Brendza, B. J. Bacskai, J. R. Cirrito, K. A. Simmons, J. M. Skoch, W. E. Klunk, C. A. Mathis, K. R. Bales, S. M. Paul, B. T. Hyman, D. M. Holtzman, *J. Clin. Invest.* **2005**, *115*, 428–433.
[78] M. Meyer-Luehmann, T. L. Spires-Jones, C. Prada, M. Garcia-Alloza, A. de Calignon, A. Rozkalne, J. Koenigsknecht-Talboo, D. M. Holtzman, B. J. Bacskai, B. T. Hyman, *Nature* **2008**, *451*, 720–724.
[79] S. Burgold, T. Bittner, M. M. Dorostkar, D. Kieser, M. Fuhrmann, G. Mitteregger, H. Kretzschmar, B. Schmidt, J. Herms, *Acta Neuropathol.* **2011**, *121*, 327–335.
[80] C. A. Mathis, N. S. Mason, B. J. Lopresti, W. E. Klunk, *Semin. Nucl. Med.* **2012**, *42*, 423–432.
[81] P. S. Vassar, C. F. Culling, *Arch. Pathol.* **1959**, *68*, 487–498.
[82] H. Naiki, K. Higuchi, M. Hosokawa, T. Takeda, *Anal. Biochem.* **1989**, *177*, 244–249.
[83] H. Levine 3rd, *Protein Sci.* **1993**, *2*, 404–410.
[84] W. E. Klunk, H. Engler, A. Nordberg, Y. Wang, G. Blomqvist, D. P. Holt, M. Bergström, I. Savitcheva, G. F. Huang, S. Estrada, B. Ausén, M. L. Debnath, J. Barletta, J. C. Price, J. Sandell, B. J. Lopresti, A. Wall, P. Koivisto, G. Antoni, C. A. Mathis, B. Långström, *Ann. Neurol.* **2004**, *55*, 306–319.
[85] M. Koole, D. M Lewis, C. Buckley, N. Nelissen, M. Vandenbulcke, D. J. Brooks, R. Vandenberghe, K. Van Laere, *J. Nucl. Med.* **2009**, *50*, 818–822.
[86] N. Nelissen, K. Van Laere, L. Thurfjell, R. Owenius, M. Vandenbulcke, M. Koole, G. Bormans, D. J. Brooks, R. Vandenberghe, *J. Nucl. Med.* **2009**, *50*, 1251–1259.
[87] R. Vandenberghe, K. Van Laere, A. Ivanoiu, E. Salmon, C. Bastin, E. Triau, S. Hasselbalch, I. Law, A. Andersen, A. Korner, L. Minthon, G. Garraux, N. Nelissen, G. Bormans, C. Buckley, R. Owenius, L. Thurfjell, G. Farrar, D. J. Brooks, *Ann. Neurol.* **2010**, *68*, 319–329.
[88] Z. Cselényi, M. E. Jönhagen, A. Forsberg, C. Halldin, P. Julin, M. Schou, P. Johnström, K. Varnäs, S. Svensson, L. Farde, *J. Nucl. Med.* **2012**, *53*, 415–424.
[89] M. Hintersteiner, A. Enz, P. Frey, A.-L. Jaton, W. Kinzy, R. Kneuer, U. Neumann, M. Rudin, M. Staufenbiel, M. Stoeckli, K.-H. Wiederhold, H.-U. Gremlich, *Nat. Biotechnol.* **2005**, *23*, 577–583.
[90] W. Yang, Y. Wong, O. T. W. Ng, L.-P. Bai, D. W. J. Kwong, Y. Ke, Z.-H. Jiang, H.-W. Li, K. K. L. Yung, M. S. Wong, *Angew. Chem. Int. Ed.* **2012**, *51*, 1804–1810; *Angew. Chem.* **2012**, *124*, 1840–1846.
[91] W. M. Chang, M. Dakanali, C. C. Capule, C. J. Sigurdson, J. Yang, E. A. Theodorakis, *ACS Chem. Neurosci.* **2011**, *2*, 249–255.
[92] K. Cao, M. Farahi, M. Dakanali, W. M. Chang, C. J. Sigurdson, E. A. Theodorakis, J. Yang, *J. Am. Chem. Soc.* **2012**, *134*, 17338–17341.
[93] K. L. Teppang, R. S. Ehrlich, J. Yang, *Methods Enzymol.* **2020**, *639*, 91–114.
[94] J. Zhou, P. Jangili, S. Son, M. S. Ji, M. Won, J. S. Kim, *Adv. Mater.* **2020**, *32*, e2001945.
[95] E. E. Nesterov, J. Skoch, B. T. Hyman, W. E. Klunk, B. J. Bacskai, T. M. Swager, *Angew. Chem. Int. Ed.* **2005**, *44*, 5452–5456; *Angew. Chem.* **2005**, *117*, 5588–5592.
[96] N. Okamura, M. Mori, S. Furumoto, T. Yoshikawa, R. Harada, S. Ito, Y. Fujikawa, H. Arai, K. Yanai, Y. Kudo, *J. Alzheimer's Dis.* **2011**, *23*, 37–48.
[97] A. Schmidt, J. Pahnke, *J. Alzheimer's Dis.* **2012**, *30*, 651–664.
[98] M. Cui, M. Ono, H. Watanabe, H. Kimura, B. Liu, H. Saji, *J. Am. Chem. Soc.* **2014**, *136*, 3388–3394.
[99] H. Fu, M. Cui, P. Tu, Z. Pan, B. Liu, *Chem. Commun.* **2014**, *50*, 11875–11878.
[100] J.-B. Li, H.-W. Liu, T. Fu, R. Wang, X.-B. Zhang, W. Tan, *Trends Chem.* **2019**, *1*, 224–234.
[101] D. H. Charych, J. O. Nagy, W. Spevak, M. D. Bednarski, *Science* **1993**, *261*, 585–588.
[102] K. P. R. Nilsson, O. Inganäs, *Nat. Mater.* **2003**, *2*, 419–424.
[103] K. Doré, S. Dubus, H–A. Ho, I. Lévesque, M. Brunette, G. Corbeil, M. Boissinot, G. Boivin, M. G. Bergeron, D. Boudreau, M. Leclerc, *J. Am. Chem. Soc.* **2004**, *126*, 4240–4244.
[104] T. Klingstedt, K. P. R. Nilsson, *Biochim. Biophys. Acta.* **2011**, *1810*, 286–296.
[105] B. Wang, B. N. Queenan, S. Wang, K. P. R. Nilsson, G. C. Bazan, *Adv. Mater.* **2019**, *31*, e1806701.
[106] K. P. R. Nilsson, J. Rydberg, L. Baltzer, O. Inganäs, *Proc. Natl. Acad. Sci. USA* **2003**, *100*, 10170–10174.
[107] K. P. R. Nilsson, J. Rydberg, L. Baltzer, O. Inganäs, *Proc. Natl. Acad. Sci. USA* **2004**, *101*, 11197–11202.
[108] K. P. R. Nilsson, A. Herland, P. Hammarström, O. Inganäs, *Biochemistry* **2005**, *44*, 3718–3724.
[109] K. P. R. Nilsson, P. Hammarström, F. Ahlgren, A. Herland, E. A. Schnell, M. Lindgren, G. T. Westermark, O. Inganäs, *ChemBioChem* **2006**, *7*, 1096–1104.
[110] C. J. -Sigurdson, K. P. R. Nilsson, S. Hornemann, G. Manco, M. Polymenidou, P. Schwarz, M. Leclerc, P. Hammarström, K. Wüthrich, A. Aguzzi, *Nat. Methods.* **2007**, *4*, 1023–1030.
[111] O. Philipson, P. Hammarström, K. P. R. Nilsson, E. Portelius, T. Olofsson, M. Ingelsson, B. T. Hyman, K. Blennow, L. Lannfelt, H. Kalimo, L. N. G. Nilsson, *Neurobiol. Aging* **2009**, *30*, 1393–1405.
[112] K. P. R. Nilsson, K. Ikenberg, A. Åslund, S. Fransson, P. Konradsson, C. Röcken, H. Moch, A. Aguzzi, *Am. J. Pathol.* **2010**, *176*, 563–574.
[113] A. Herland, K. P. R. Nilsson, J. D. Olsson, P. Hammarström, P. Konradsson, O. Inganäs, *J. Am. Chem. Soc.* **2005**, *127*, 2317–2323.

[114] K. P. R. Nilsson, A. Åslund, I. Berg, S. Nyström, P. Konradsson, A. Herland, O. Inganäs, F. Stabo-Eeg, M. Lindgren, G. T. Westermark, L. Lannfelt, L. N. Nilsson, P. Hammarström, *ACS Chem. Biol.* **2007**, *2*, 553–560.
[115] A. Åslund, C. J. Sigurdson, T. Klingstedt, S. Grathwohl, T. Bolmont, D. L. Dickstein, E. Glimsdal, S. Prokop, M. Lindgren, P. Konradsson, D. M. Holtzman, P. R. Hof, F. L. Heppner, S. Gandy, M. Jucker, A. Aguzzi, P. Hammarström, K. P. R. Nilsson, *ACS Chem. Biol.* **2009**, *4*, 673–684.
[116] V. Mahajan, T. Klingstedt, R. Simon, K. P. R. Nilsson, A. Thueringer, K. Kashofer, J. Haybaeck, H. Denk, P. M. Abuja, K. Zatloukal, *Gastroenterology* **2011**, *141*, 1080–1090.
[117] T. Klingstedt, A. Åslund, R. A. Simon, L. B. G. Johansson, J. J. Mason, S. Nyström, P. Hammarström, K. P. R. Nilsson, *Org. Biomol. Chem.* **2011**, *9*, 8356–8370.
[118] T. Klingstedt, H. Shirani, K. O. A. Åslund, N. J. Cairns, C. J. Sigurdson, M. Goedert, K. P. R. Nilsson, *Chem. Eur. J.* **2013**, *19*, 10179–10192.
[119] L. B. G. Johansson, R. Simon, G. Bergström, M. Eriksson, S. Prokop, C. F. Mandenius, F. L. Heppner, K. O. A. Åslund, K. P. R. Nilsson, *Biosens. Bioelectron.* **2015**, *63*, 204–211.
[120] R. A. Simon, H. Shirani, K. O. A. Åslund, M. Bäck, V. Haroutunian, S. Gandy, K. P. R. Nilsson, *Chem. Eur. J.* **2014**, *20*, 12537–12543.
[121] T. Klingstedt, H. Shirani, J. Mahler, B. M. Wegenast-Braun, S. Nyström, M. Goedert, M. Jucker, K. P. R. Nilsson, *Chem. Eur. J.* **2015**, *21*, 9072–9082.
[122] U. S. Herrmann, A. K. Schütz, H. Shirani, D. Huang, D. Saban, M. Nuvolone, B. Li, B. Ballmer, K. O. A. Åslund, J. J. Mason, E. Rushing, H. Budka, S. Nyström, P. Hammarström, A. Böckmann, A. Caflisch, B. H. Meier, K. P. R. Nilsson, S. Hornemann, A. Aguzzi, *Sci. Transl. Med.* **2015**, *7*, 299ra123.
[123] K. Magnusson, R. Simon, D. Sjölander, C. J. Sigurdson, P. Hammarström, K. P. R. Nilsson, *Prion* **2014**, *8*, 319–329.
[124] H. Shirani, M. Linares, C. J. Sigurdson, M. Lindgren, P. Norman, K. P. R. Nilsson, *Chem. Eur. J.* **2015**, *21*, 15133–15137.
[125] L. Lantz, H. Shirani, T. Klingstedt, K. P. R. Nilsson, *Chem. Eur. J.* **2020**, *26*, 7425–7432.
[126] C. Gustafsson, H. Shirani, P. Leira, D. R. Rehn, M. Linares, K. P. R. Nilsson, P. Norman, M. Lindgren, *ChemPhysChem* **2021**, *22*, 323–335.
[127] L. Björk, M. Bäck, L. Lantz, B. Ghetti, R. Vidal, T. Klingstedt, K. P. R. Nilsson, *Chem. Eur. J.* **2022**, *28*, e202201557.
[128] C. J. Sigurdson, K. P. R. Nilsson, S. Hornemann, M. Heikenwalder, G. Manco, P. Schwarz, D. Ott, T. Rülicke, P. P. Liberski, C. Julius, J. Falsig, L. Stitz, K. Wüthrich, A. Aguzzi, *Proc. Natl. Acad. Sci. USA* **2009**, *106*, 304–309.
[129] C. J. Sigurdson, K. P. R. Nilsson, S. Hornemann, G. Manco, N. Fernández-Borges, P. Schwarz, J. Castilla, K. Wüthrich, A. Aguzz, *J. Clin. Invest.* **2010**, *120*, 2590–2599.
[130] K. P. R. Nilsson, S. Joshi-Barr, O. Winson, C. J. Sigurdson, *J. Neurosci.* **2010**, *30*, 12094–12102.
[131] C. J. Sigurdson, S. Joshi-Barr, C. Bett, O. Winson, G. Manco, P. Schwarz, T. Rülicke, K. P. R. Nilsson, I. Margalith, A. Raeber, D. Peretz, S. Hornemann, K. Wüthrich, A. Aguzzi, *J. Neurosci.* **2011**, *31*, 13840–13847.
[132] C. Bett, N. Fernández-Borges, T. D. Kurt, M. Lucero, K. P. R. Nilsson, J. Castilla, C. J. Sigurdson, *FASEB J.* **2012**, *26*, 2868–2876.
[133] C. Bett, T. D. Kurt, M. Lucero, M. Trejo, A. J. Rozemuller, Q. Kong, K. P. R. Nilsson, E. Masliah, M. B. Oldstone, C. J. Sigurdson, *PLoS Pathog.* **2013**, *9*, e1003280.
[134] P. Aguilar-Calvo, X. Xiao, C. Bett, H. Eraña, K. Soldau, J. Castilla, K. P. R. Nilsson, W. K. Surewicz, C. J. Sigurdson, *Sci. Rep.* **2017**, *8*, 43295.
[135] P. Hammarström, R. Simon, S. Nyström, P. Konradsson, A. Åslund, K. P. R. Nilsson, *Biochemistry* **2010**, *49*, 6838–6845.
[136] A. L. Göransson, K. P. R. Nilsson, K. Kågedal, A. C. Brorsson, *Biochem. Biophys. Res. Commun.* **2012**, *420*, 895–900.
[137] I. Berg, K. P. R. Nilsson, S. Thor, P. Hammarström, *Nat. Protoc.* **2010**, *5*, 935–944.
[138] S. W. Schultz, K. P. R. Nilsson, G. T. Westermark, *PLoS One* **2011**, *6*, e20221.
[139] I. Caesar, M. Jonson, K. P. R. Nilsson, S. Thor, P. Hammarström, *PLoS One* **2012**, *7*, e31424.
[140] T. Klingstedt, C. Blechschmidt, A. Nogalska, S. Prokop, B. Häggqvist, O. Danielsson, W. K. Engel, V. Askanas, F. L. Heppner, K. P. R. Nilsson, *ChemBioChem* **2013**, *14*, 607–616.
[141] T. Klingstedt, B. Ghetti, J. L. Holton, H. Ling, K. P. R. Nilsson, M. Goedert, *Acta. Neuropathol. Commun.* **2019**, *7*, 193.
[142] W. Becker, *J. Microsc.* **2012**, *247*, 119–136.
[143] P. Aguilar-Calvo, C. Bett, A. M. Sevillano, T. D. Kurt, J. Lawrence, K. Soldau, P. Hammarström, K. P. R. Nilsson, C. J. Sigurdson, *Brain Pathol.* **2018**, *28*, 999–1011.
[144] P. Aguilar-Calvo, A. M. Sevillano, J. Bapat, K. Soldau, D. R. Sandoval, H. C. Altmeppen, L. Linsenmeier, D. P. Pizzo, M. D. Geschwind, H. Sanchez, B. S. Appleby, M. L. Cohen, J. G. Safar, S. D. Edland, M. Glatzel, K. P. R. Nilsson, J. D. Esko, C. J. Sigurdson, *Acta Neuropathol.* **2020**, *139*, 527–546.
[145] A. M. Sevillano, P. Aguilar-Calvo, T. D. Kurt, J. A. Lawrence, K. Soldau, T. H. Nam, T. Schumann, D. P. Pizzo, S. Nyström, B. Choudhury, H. Altmeppen, J. D. Esko, M. Glatzel, K. P. R. Nilsson, C. J. Sigurdson, *J. Clin. Invest.* **2020**, *130*, 1350–1362.
[146] J. D. Ulrich, T. K. Ulland, T. E. Mahan, S. Nyström, K. P. R. Nilsson, W. M. Song, Y. Zhou, M. Reinartz, S. Choi, H. Jiang, F. R. Stewart, E. Anderson, Y. Wang, M. Colonna, D. M. Holtzman, *J. Exp. Med.* **2018**, *215*, 1047–1058.
[147] L. Lantz, H. Shirani, B. Ghetti, R. Vidal, T. Klingstedt, K. P. R. Nilsson, *Chem. Eur. J.* **2023**, *29*, e202203568.
[148] A. Lord, O. Philipson, T. Klingstedt, G. Westermark, P. Hammarström, K. P. R. Nilsson, L. N. Nilsson, *Am. J. Pathol.* **2011**, *178*, 2286–2298.
[149] S. Solé-Domènech, P. Sjövall, V. Vukojević, R. Fernando, A. Codita, S. Salve, N. Bogdanović, A. H. Mohammed, P. Hammarström, K. P. R. Nilsson, F. M. LaFerla, S. Jacob, P. O. Berggren, L. Giménez-Llort, M. Schalling, L. Terenius, B. Johansson, *Acta Neuropathol.* **2013**, *125*, 145–157.
[150] S. K. Fritschi, A. Cintron, L. Ye, J. Mahler, A. Bühler, F. Baumann, M. Neumann, K. P. R. Nilsson, P. Hammarström, L. C. Walker, M. Jucker, *Acta Neuropathol.* **2014**, *128*, 477–484.
[151] J. Mahler, J. Morales-Corraliza, J. Stolz, A. Skodras, R. Radde, C. C. Duma, Y. S. Eisele, M. J. Mazzella, H. Wong, W. E. Klunk, K. P. R. Nilsson, M. Staufenbiel, P. M. Mathews, M. Jucker, B. M. Wegenast-Braun, *Neurobiol. Aging.* **2015**, *36*, 2241–2247.
[152] T. H. Chu, K. Cummins, J. S. Sparling, S. Tsutsui, C. Brideau, K. P. R. Nilsson, J. T. Joseph, P. K. Stys, *PLoS One.* **2017**, *12*, e0188218.
[153] J. Wagner, K. Degenhardt, M. Veit, N. Louros, K. Konstantoulea, A. Skodras, K. Wild, P. Liu, U. Obermüller, V. Bansal, A. Dalmia, L. M. Häsler, M. Lambert, M. De Vleeschouwer, H. A. Davies, J. Madine, D. Kronenberg-Versteeg, R. Feederle, D. Del Turco, K. P. R. Nilsson, T. Lashley, T. Deller, M. Gearing, L. C. Walker, P. Heutink, F. Rousseau, J. Schymkowitz, M. Jucker, J. J. Neher, *Nature* **2022**, *612*, 123–131.
[154] G. Tanriöver, M. Bacioglu, M. Schweighauser, J. Mahler, B. M. Wegenast-Braun, A. Skodras, U. Obermüller, M. Barth, D. Kronenberg-Versteeg, K. P. R. Nilsson, D. R. Shimshek, P. J. Kahle, Y. S. Eisele, M. Jucker, *Acta Neuropathol. Commun.* **2020**, *8*, 133.
[155] A. Stepanchuk, W. Tahir, K. P. R. Nilsson, H. M. Schatzl, P. K. Stys, *J. Neurochem.* **2021**, *156*, 1033–1048.
[156] A. Ruiz-Riquelme, A. Mao, M. M. Barghash, H. H. C. Lau, E. Stuart, G. G. Kovacs, K. P. R. Nilsson, P. E. Fraser, G. Schmitt-Ulms, J. C. Watts, *Acta Neuropathol. Commun.* **2021**, *9*, 83.
[157] D. Sjölander, J. Bijzet, B. P. Hazenberg, K. P. R. Nilsson, P. Hammarström, *Amyloid* **2015**, *22*, 19–25.
[158] Y. Sekijima, R. I. Campos, P. Hammarström, K. P. R. Nilsson, T. Yoshinaga, K. Nagamatsu, M. Yazaki, F. Kametani, S. J. Ikeda, *Peripher. Nerv. Syst.* **2015**, *20*, 372–379.
[159] D. Sjölander, C. Röcken, P. Westermark, G. T. Westermark, K. P. R. Nilsson, P. Hammarström, *Amyloid* **2016**, *23*, 98–108.
[160] K. Hahn, K. P. R. Nilsson, P. Hammarström, P. Urban, R. R. Meliss, H. M. Behrens, S. Krüger, C. Röcken, *Amyloid* **2017**, *24*, 78–86.
[161] M. Shahnawaz, A. Mukherjee, S. Pritzkow, N. Mendez, P. Rabadia, X. Liu, B. Hu, A. Schmeichel, W. Singer, G. Wu, A. L. Tsai, H. Shirani, K. P. R. Nilsson, P. A. Low, C. Soto, *Nature* **2020**, *578*, 273–277.
[162] S. Nyström, A. Vahdat Shariat Panahi, K. P. R. Nilsson, P. Westermark, G. T. Westermark, P. Hammarström, K. Lundmark, *Amyloid* **2017**, *24*, 140–141.
[163] H. Liu, C. Kim, T. Haldiman, C. J. Sigurdson, S. Nyström, K. P. R. Nilsson, M. L. Cohen, T. Wisniewski, P. Hammarström, J. G. Safar, *J. Biol. Chem.* **2021**, *297*, 101267.
[164] M. Jonson, S. Nyström, A. Sandberg, M. Carlback, W. Michno, J. Hanrieder, A. Starkenberg, K. P. R. Nilsson, S. Thor, P. Hammarström, *Cell Chem. Biol.* **2018**, *25*, 595–610.e5.
[165] W. Michno, I. Kaya, S. Nyström, L. Guerard, K. P. R. Nilsson, P. Hammarström, K. Blennow, H. Zetterberg, J. Hanrieder, *Anal. Chem.* **2018**, *90*, 8130–8138.
[166] W. Michno, S. Nyström, P. Wehrli, T. Lashley, G. Brinkmalm, L. Guerard, S. Syvänen, D. Sehlin, I. Kaya, D. Brinet, K. P. R. Nilsson, P.

Hammarström, K. Blennow, H. Zetterberg, J. Hanrieder, *J. Biol. Chem.* **2019**, *294*, 6719–6732.
[167] K. M. Psonka-Antonczyk, P. Hammarström, L. B. G. Johansson, M. Lindgren, B. T. Stokke, K. P. R. Nilsson, S. Nyström, *Front. Chem.* **2016**, *4*, 44.
[168] D. Kirschenbaum, E. Dadgar-Kiani, F. Catto, F. F. Voigt, C. Trevisan, O. Bichsel, H. Shirani, K. P. R. Nilsson, K. J. Frontzek, P. Paganetti, F. Helmchen, J. Hyung Lee, A. Aguzzi, *EMBO Mol. Med.* **2022**, e16789.
[169] J. Brelstaff, B. Ossola, J. J. Neher, T. Klingstedt, K. P. R. Nilsson, M. Goedert, M. G. Spillantini, A. M. Tolkovsky, *Front. Neurol. Neurosci.* **2015**, *9*, 184.
[170] B. M. Wegenast-Braun, A. Skodras, G. Bayraktar, J. Mahler, S. K. Fritschi, T. Klingstedt, J. J. Mason, P. Hammarström, K. P. R. Nilsson, C. Liebig, M. Jucker, *Am. J. Pathol.* **2012**,*181*, 1953–1960.
[171] R. Ni, Z. Chen, J. A. Gerez, G. Shi, Q. Zhou, R. Riek, K. P. R. Nilsson, D. Razansky, J. Klohs, *Biomed. Opt. Express.* **2020**, *11*, 4989–5002.
[172] M. Calvo-Rodriguez, S. S. Hou, A. C. Snyder, S. Dujardin, H. Shirani, K. P. R. Nilsson, B. J. Bacskai, *Acta Neuropathol. Commun.* **2019**, *7*, 171.
[173] R. Ni, Z. Chen, X. L. Deán-Ben, F. F. Voigt, D. Kirschenbaum, G. Shi, A. Villois, Q. Zhou, A. Crimi, P. Arosio, R. M. Nitsch, K. P. R. Nilsson, A. Aguzzi, F. Helmchen, J. Klohs, D. Razansky, *Nat. Biomed. Eng.* **2022**, *6*, 1031–1044.
[174] P. Nordeman, L. B. G. Johansson, M. Bäck, S. Estrada, H. Hall, D. Sjölander, G. T. Westermark, P. Westermark, L. Nilsson, P. Hammarström, K. P. R. Nilsson, G. Antoni, *ACS Med. Chem. Lett.* **2016**, *7*, 368–373.
[175] A. K. Schütz, S. Hornemann, M. A. Wälti, L. Greuter, C. Tiberi, R. Cadalbert, M. Gantner, R. Riek, P. Hammarström, K. P. R. Nilsson, A. Böckmann, A. Aguzzi, B. H. Meier, *ACS Chem. Neurosci.* **2018**, *9*, 475–481.
[176] C. König, R. Skånberg, I. Hotz, A. Ynnerman, P. Norman, M. Linares, *Chem. Commun. (Camb.)* **2018**, *54*, 3030–3033.
[177] J. Sjöqvist, J. Maria, R. A. Simon, M. Linares, P. Norman, K. P. R. Nilsson, M. Lindgren, *J. Phys. Chem. A.* **2014**, *118*, 9820–9827.
[178] C. Gustafsson, M. Linares, P. Norman, *J. Phys. Chem. A.* **2020**, *124*, 875–888.
[179] M. Bäck, H. Appelqvist, H. LeVine 3rd, K. P. R. Nilsson, *Chem. Eur. J.* **2016**, *22*, 18335–18338.
[180] K. P. R. Nilsson, M. R. Andersson, O. Inganäs, *J. Phys. Condens. Matter* **2002**, *14*, 10011–10020.
[181] G. W. Small, V. Kepe, L. M. Ercolim, P. Siddarth, S. Y. Bookheimer, K. J. Miller, H. Lavretsky, A. C. Burggren, G. M. Cole, H. V. Vinters, P. M. Thompson, S. C. Huang, N. Satyamurthy, M. E. Phelps, J. R. Barrio, *N. Eng. J. Med.* **2006**, *355*, 2652–2663.
[182] A. Taghavi, S. Nasir, M. Pickhardt, R. Heyny-von Haussen, G. Mall, E. Mandelkow, E. M. Mandelkow, B. Schmidt, *J. Alzheimer's Dis.* **2011**, *27*, 835–843.
[183] M. T. Fodero-Tavoletti, N. Okamura, S. Furumoto, R. S. Mulligan, A. R. Connor, C. A. McLean, D. Cao, A. Rigopoulos, G. A. Cartwright, G. O'Keefe, S. Gong, P. A. Adlard, K. J. Barnham, C. C. Rowe, C. L. Masters, Y. Kudo, R. Cappai, K. Yanai, V. L. Villemagne, *Brain* **2011**, *134*, 1089–1100.
[184] W. Zhang, J. Arteaga, D. K. Cashion, G. Chen, U. Gangadharmath, L. F. Gomez, D. Kasi, C. Lam, Q. Liang, C. Liu, V. P. Mocharla, F. Mu, A. Sinha, A. K. Szardenings, E. Wang, J. C. Walsh, C. Xia, C. Yu, T. Zhao, H. C. Kolb, *J. Alzheimer's Dis.* **2012**, *31*, 601–612.
[185] M. Maruyama, H. Shimada, T. Suhara, H. Shinotoh, B. Ji, J. Maeda, M. R. Zhang, J. Q. Trojanowski, V. M. Lee, M. Ono, K. Masamoto, H. Takano, N. Sahara, N. Iwata, N. Okamura, S. Furumoto, Y. Kudo, Q. Chang, T. C. Saido, A. Takashima, J. Lewis, M. K. Jang, I. Aoki, H. Ito, M. Higuchi, *Neuron* **2013**, *79*, 1094–1108.
[186] C. F. Xia, J. Arteaga, G. Chen, U. Gangadharmath, L. F. Gomez, D. Kasi, C. Lam, Q. Liang, C. Liu, V. P. Mocharla, F. Mu, A. Sinha, H. Su, A. K. Szardenings, J. C. Walsh, E. Wang, C. Yu, W. Zhang, T. Zhao, H. C. Kolb, *Alzheimer's Dementia* **2013**, *9*, 666–676.
[187] R. Harada, N. Okamura, S. Furumoto, T. Tago, K. Yanai, H. Arai, Y. Kudo, *Biomol. Eng.* **2016**, *6*, 7.
[188] A. M. Walji, E. D. Hostetler, H. Selnick, Z. Zeng, P. Miller, I. Bennacef, C. Salinas, B. Connolly, L. Gantert, M. Holahan, S. O'Malley, M. Purcell, K. Riffel, J. Li, J. Balsells, J. A. OBrien, S. Melquist, A. Soriano, X. Zhang, A. Ogawa, S. Xu, E. Joshi, J. Della Rocca, F. J. Hess, J. Schachter, D. Hesk, D. Schenk, A. Struyk, K. Babaoglu, T. G. Lohith, Y. Wang, K. Yang, J. Fu, J. L. Evelhoch, P. J. Coleman, *J. Med. Chem.* **2016**, *59*, 4778–4789.
[189] C. Aguero, M. Dhaynaut, M. D. Normandin, A. C. Amaral, N. J. Guehl, R. Neelamegam, M. Marquie, K. A. Johnson, G. El Fakhri, M. P. Frosch, T. Gómez-Isla, *Acta Neuropathol.* **2019**, *7*, 37.
[190] V. L. Villemagne, M. Fodero-Tavoletti, C. L. Masters, C. C. Rowe, *Lancet Neurol.* **2015**, *14*, 114–124.
[191] L. Lemoine, P. G. Gillberg, M. Svedberg, V. Stepanov, Z. Jia, J. Huang, S. Nag, H. Tian, B. Ghetti, N. Okamura, M. Higuchi, C. Halldin, A. Nordberg, *Alzheimer's Res. Ther.* **2017**, *9*, 96.
[192] A. Leuzy, K. Chiotis, L. Lemoine, P–G. Gillberg, O. Almkvist, E. Rodriguez-Vieitez, A. Nordberg, *Mol. Psychiatry* **2019**, *24*, 1112–1134.
[193] K. P. Ng, T. A. Pascoal, S. Mathotaarachchi, J. Therriault, M. S. Kang, M. Shin, M–C. Guiot, Q. Guo, R. Harada, R. A. Comley, G. Massarweh, J–P. Soucy, N. Okamura, S. Gauthier, P. Rosa-Neto, *Alzheimer's Res. Ther.* **2017**, *9*, 25.
[194] C. Vermeiren, P. Motte, D. Viot, G. Mairet-Coello, J–P. Courade, M. Citron, J. Mercier, J. Hannestad, M. Gillard, *Mov. Disord.* **2018**, *33*, 272–281.
[195] Š. Korat, N. S. R. Bidesi, F. Bonanno, A. Di Nanni, A. N. N. Hoàng, K. Herfert, A. Maurer, U. M. Battisti, G. D. Bowden, D. Thonon, D. Vugts, A. D. Windhorst, M. M. Herth, *Pharmaceuticals (Basel)* **2021**,*14*, 847.
[196] H. Shirani, H. Appelqvist, M. Bäck, T. Klingstedt, N. J. Cairns, K. P. R. Nilsson, *Chem. Eur. J.* **2017**, *23*, 17127–17135.
[197] T. Klingstedt, H. Shirani, B. Ghetti, R. Vidal, K. P. R. Nilsson, *ChemBioChem.* **2021**, *22*, 2568–2581.
[198] Y. Todarwal, C. Gustafsson, N. N. Thi Minh, I. Ertzgaard, T. Klingstedt, B. Ghetti, R. Vidal, C. König, M. Lindgren, K. P. R. Nilsson, M. Linares, P. Norman, *J. Phys. Chem. B* **2021**, *125*, 11628–11636.
[199] M. Ramesh, A. Acharya, N. A. Murugan, H. Ila, T. Govindaraju, *ChemBioChem* **2021**, *22*, 3348–3357.

Manuscript received: January 20, 2023
Revised manuscript received: March 3, 2023
Accepted manuscript online: March 9, 2023
Version of record online: May 8, 2023